RESEARCH ARTICLE

Geoarchaeology An International Journal   WILEY

Mid- to late Holocene environmental changes and human-environment interactions in the surroundings of La Silla del Papa, SW Spain

Simon M. May[1] ⓘ | Maike Norpoth[1] | Anna Pint[1] | Lyudmila Shumilovskikh[2,3] |
Kira Raith[4] | Dominik Brill[1] | Gilles Rixhon[5] | Pierre Moret[6] |
Helena Jiménez-Vialás[6,7] | Ignasi Grau-Mira[8] | Iván García-Jiménez[9] |
Dirce Marzoli[10] | César León-Martín[10] | Klaus Reicherter[11] | Helmut Brückner[1] ⓘ

[1]Institute of Geography, University of Cologne, Cologne, Germany

[2]Department of Palynology and Climate Dynamics, Albrecht-von-Haller-Institute for Plant Sciences, Georg-August-University Göttingen, Göttingen, Germany

[3]Tomsk State University, Tomsk, Russia

[4]Department of Social Sciences, Human Origins and Palaeoenvironments Research Group, Oxford Brookes University, Oxford, UK

[5]Laboratoire Image Ville Environnement (LIVE), Faculté de géographie et d'aménagement, Ecole Nationale du Génie de l'Eau et de l'Environnement (ENGEES), Université de Strasbourg, Strasbourg, France

[6]Laboratoire TRACES – UMR 5608 du CNRS, Université de Toulouse, Toulouse, France

[7]University of Murcia, Campus La Merced, Spain

[8]University of Alicante, Sant Vicent del Raspeig, Spain

[9]Conjunto Arqueológico de Baelo Claudia, Área de Investigación y Conservación, Tarifa, Cádiz, Spain

[10]Department of Madrid, German Archaeological Institute, Madrid, Spain

[11]Neotectonics and Natural Hazards, RWTH Aachen University, Aachen, Germany

Correspondence
Simon Matthias May, Institute of Geography, University of Cologne, 50923 Cologne, Germany.
Email: mays@uni-koeln.de

Funding information
Deutsche Forschungsgemeinschaft; Agence Nationale de la Recherche

Abstract

In southern Iberia, the surroundings of the Strait of Gibraltar are known as a crossroad for population movements, cultural exchange, and trade from Late Pre-history to modern times. However, questions remain about the impact of this historical development on the environment. The settlement of La Silla del Papa, an important hillfort in southern Andalusia (Cádiz), was occupied during the entire Iron Age, replaced by the coastal town Baelo Claudia during Roman times, and re-occupied during Early Medieval times. As such, La Silla del Papa and its territory represent an ideal location for long-term studies on human-environment interactions. Within the framework of the interdisciplinary project "Archeostraits," geoarchaeological investigations in the surroundings of La Silla del Papa aimed at constraining ecological conditions and human-environment interactions during the

Scientific editing by Kevin Walsh.

mid- and late Holocene and during major human occupation phases. Our results document an early mid-Holocene marine embayment in the lower floodplain of the Río del Cachón, rapidly turning into a coastal lagoon and later into freshwater-dominated wetlands. After approximately 2100 BP (c. 150 BC), fluvial and alluvial deposition increased, suggesting a high anthropogenic impact on the local landscape during Roman or post-Roman times. Palynological results reveal fluctuating agricultural and pastoral activities and distinct periods of landscape opening during the Neolithic and Iron Age.

KEYWORDS

Archeostraits project, Baelo Claudia, coastal changes, La Silla del Papa, microfaunal investigation, palynological analyses, sea-level evolution, soil erosion, Zahara de los Atunes

1 | INTRODUCTION

Mediterranean landscapes are generally thought to have experienced considerable degradation during the Holocene (Bellin et al., 2013; Cammeraat & Imeson, 1998; Thornes & Brandt, 1996; Thornes & Wainwright, 2004), expressed in high rates of soil erosion documented in a variety of geo-bio-archives. However, it remains much debated whether the key drivers for these environmental changes were climatic changes, that is, aridification during the mid-Holocene (Jalut et al., 2009; Petit-Maire, 1990), human impact (Brückner, 1986), or the combination of both (van Andel and Zangger, 1990; Bellin et al., 2013; Brückner et al., 2017; Burillo-Mozota et al., 1986; Fuchs et al., 2004; Fuchs, 2007; Roberts, 1990; Roberts et al., 2004; 2011; Schulte, 2002; Shumilovskikh et al., 2016; Vita-Finzi, 1969; Wainwright, 1994; Wolf & Faust, 2015). According to Roberts et al. (2011), it is not questionable whether human impact influenced the Mediterranean landscape, but when the impact became detectable and to what extent. In this regard, the understanding of past human-environment interactions will contribute to the projection of present and future challenges resulting from the interplay of anthropogenic impact, climate change, and soil erosion.

In southern Spain, palaeoenvironmental changes such as changing vegetation patterns and fluctuating soil erosion generally occurred contemporary to the presence of human communities, although the timing of notable anthropogenic impact remains unclear. For instance, Schröder et al. (2018) report on humid conditions and highest lake levels between 7800 and 5500 BP based on a multiproxy study at Lake Medina (SW Spain), which is followed by progressive aridification, the establishment of typical Mediterranean-type vegetation, and an increasing anthropogenic impact during the last two millennia. Similarly, Carrión et al. (2010) suggest an only insignificant impact of agricultural activities on the landscape in SE Spain during pre-Roman times, and a maximum of anthropogenic disturbance during and after the Roman Empire. In contrast, Castro et al. (1998) and López-Sáez et al. (2002) infer notable human-induced landscape degradation and desertification in SE and SW Spain already between 6000 BP and 500 BP.

Of particular interest are the specific variations of these phenomena in the Campo de Gibraltar district, at the southernmost tip of the Iberian Peninsula. On the one hand, this area is compartmentalized by a complex system of mountain ranges, leaving only a narrow habitable zone between the mountains and the coast. On the other hand, the Strait of Gibraltar has made it a crossroad for population movements, cultural exchanges, and trade from Prehistory to recent times (Coltelloni-Trannoy et al., 2016). Until the Early Middle Ages, five major human occupation phases related to increased human pressure on the landscape can be identified, which are likely to have had a measurable impact on the Holocene environment in this area. Deciphering the influence of these historical transitions on landscape changes is challenging, that is, questions remain whether agricultural patterns have significantly altered due to political crises, cultural changes or technical innovations. Studying palaeoenvironmental changes in the vicinity of these settlements is therefore crucial for unraveling the consequences of settlement locations and farming strategies for local environmental conditions (Buxó, 2008).

For this purpose, geoarchaeological investigations were performed in the surroundings of two of the most important Iron Age settlements in southern Iberia, La Silla del Papa in Cádiz Province (Moret & Prados-Martínez, 2014; Moret et al., 2010, 2014, 2017) and Los Castillejos de Alcorrín in Málaga Province (Marzoli et al., 2009, 2010, 2014; Marzoli, 2012; Renzi et al., 2014, 2016; Figure 1), both subject to archaeological investigations during the recent past. This article presents results from investigations on the Atlantic side of this interdisciplinary research project "Archeostraits." Located approximately 20 km northwest of the Strait of Gibraltar at the south-eastern end of the Gulf of Cádiz (Andalusia; Figure 2), La Silla del Papa was the central place of a territory which probably covered the bays of Bolonia and of Zahara. Archaeological investigations documented that this hillfort was occupied from approximately 900 to 25 BC (Moret et al., 2010), then replaced by the coastal town of Baelo Claudia until approximately 600 AD (Moret & Prados-Martínez, 2014; Sillières, 1997), and then re-occupied until approximately 900 AD (Gutiérrez-Lloret et al., 2017), while rural
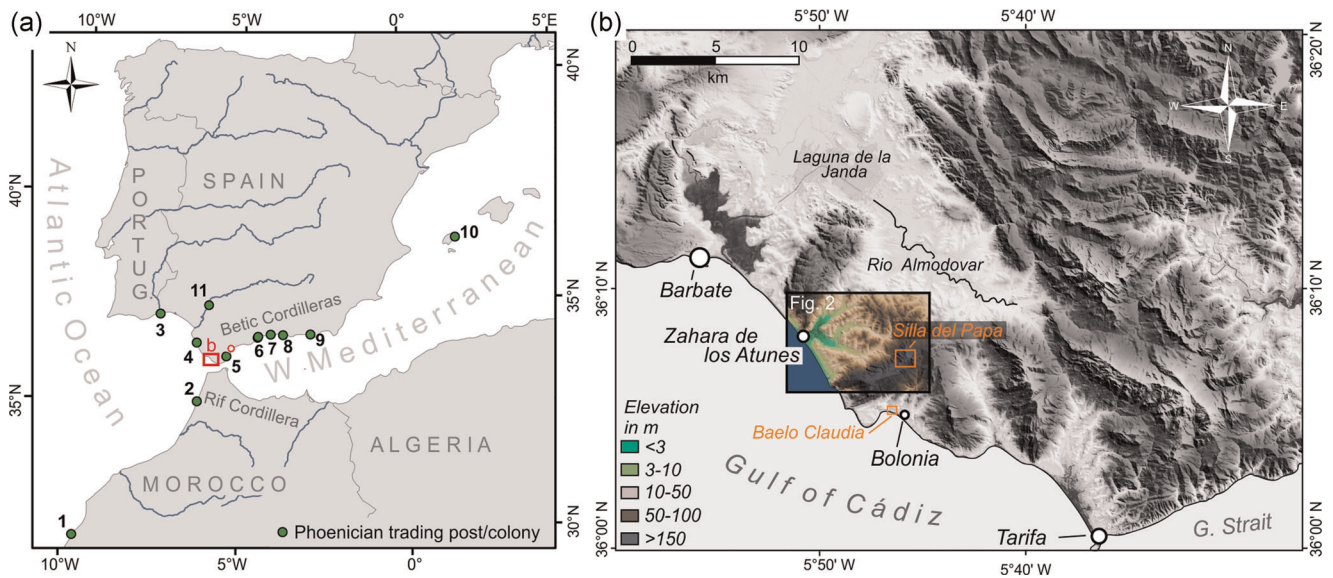
FIGURE 1 Overview and location of the study area. (a) Location of the study area in SW Spain with important Phoenician colonies and trading posts. 1 – Mogador; 2 – Lixus; 3 – Ayamonte; 4 – Gadir; 5 – Carteia; 6 – Malaka; 7 – Sexi; 8 – Selambina; 9 – Abdera; 10 – Ebusus; 11 – Sevilla-Hispalis (based on Aubet, 2001; Klein et al., 2016; Tsetskhladze, 2006). Location of Los Castillejos de Alcorrín, an important Iron Age settlement in the Mediterranean area (e.g., Marzoli et al., 2010), is depicted as well (small red circle). (b) Regional setting and location of the study area, that is, the catchment of the Río del Cachón. La Silla del Papa (Bailo), the Iron Age predecessor of Roman Baelo Claudia, is located on top of the Sierra de la Plata; Baelo Claudia was founded around 40–20 BC when its predecessor settlement Bailo was abandoned (e.g., Moret et al., 2008, 2017) [Color figure can be viewed at wileyonlinelibrary.com]

settlements also changed according to the location of the town (Jiménez-Vialás & Grau-Mira, 2019). The research was carried out in the catchment of the Río del Cachón, which rises in the Sierra de la Plata directly below the Iron Age settlement of La Silla del Papa (Arroyo del Candalar), and debouches into the Atlantic Ocean at Zahara de los Atunes (Figure 2). Based on sedimentological, geochemical, chronological (OSL, ^{14}C-AMS, and diagnostic pottery), microfaunal and palynological analyses of nine sediment profiles in the transitional reaches of the catchment as well as nine vibracores from the lower floodplain section and the estuary, this study aims at (i) investigating the environmental and coastal changes in the surroundings of La Silla del Papa during the mid- and late Holocene; (ii) constraining environmental conditions during the major human occupation phases, particularly the period of early Phoenician colonization; and (iii) deciphering extent and timing of local human-environment interactions in the river catchment, which may be related to the occupation of La Silla del Papa and/or the population dynamics in its territory.

2 | REGIONAL SETTING

### 2.1 | Geological and geomorphological setting

Within the active convergence zone between the African and Eurasian plates, the study area is located in the westernmost part of the Betic Cordilleras (Grützner et al., 2012; Figure 1). Stretching from the southeastern Iberian Peninsula to Morocco (Rif Cordilleras;

Gibbons & Moreno, 2002; González-Castillo et al., 2015), the mountain range has evolved in the context of the Alpine orogeny from the Late Cretaceous onwards (Gibbons & Moreno, 2002; Grützner et al., 2012; Vergés & Fernández, 2012).

As part of the Gibraltar Flysch Zone, the study area is mainly composed of the Late Cretaceous Almarchal Formation (limestones, marl- and claystones) and the folded Miocene Aljibe Formation (sandstone; Figure 3). Diverse postorogenic Miocene to Late Quaternary deposits (alluvial and colluvial sediments, marine terraces) also occur (Figure 3). The coastal area of Zahara de los Atunes is enclosed by two transpressive faults along the Sierra de Retín (316 m asl) to the north and the Sierra de la Plata (459 m asl) to the south (Silva et al., 2006). Based on displacements of the MIS 5 marine terraces (i.e., elevations of + 14 and + 3 m asl for the 5e and 5c terraces, respectively) and an overall S-N decreasing uplift gradient from the Strait of Gibraltar towards Cádiz, estimated peak uplift rates amount to 0.15 mm/a in our study area during the Late Quaternary (Zazo et al., 1999, 2008). Although neotectonic data from the study area are generally rare, mid-Holocene activity of the Carrizales Fault in the Sierra de la Plata was documented by Grützner et al. (2010, 2012). According to these authors, active faulting in the study area takes place along N–S trending normal faults at present, although strain rates are generally slow, suggesting that faults should generally be slow moving.

The Arroyo del Candalar, Arroyo del Acebuchal and Arroyo de la Zarzuela join downstream to form the Río del Cachón; together they drain an area of c. 39.5 km² (Figure 2a). Headwaters of the Arroyo del Candalar originate on the northern hillslopes of the Sierra de la Plata,
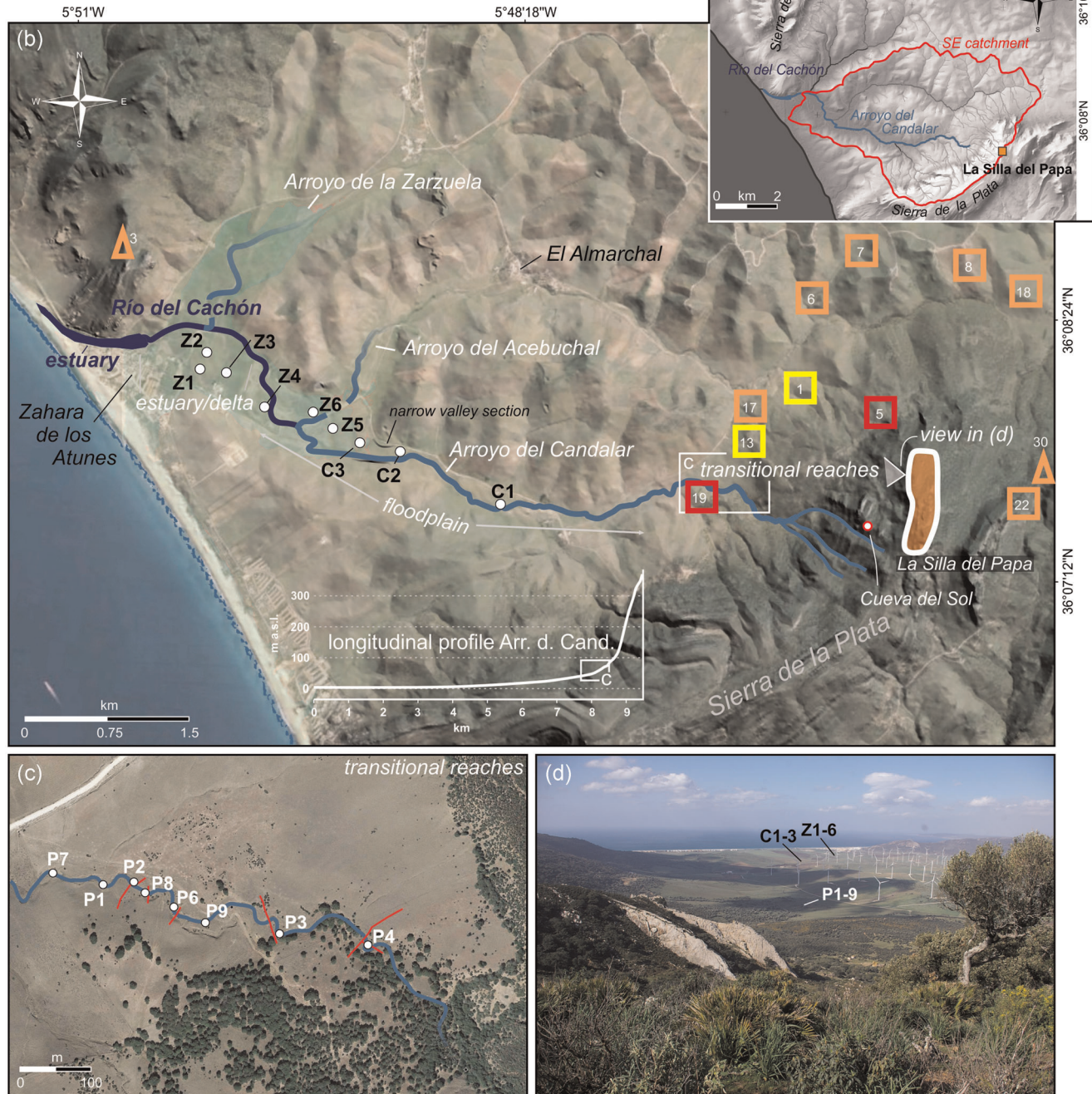
FIGURE 2 Setting and overview of the study area. (a) The catchment of the Río del Cachón, debouching into the Atlantic Ocean close to Zahara de los Atunes; boundary of the arroyos del Candalar and del Acebuchal sub-catchment is marked by red line ("SE catchment"). (b) Overview of the catchment of the Arroyo del Candalar, including locations of sediment cores in the lower floodplain and relevant archaeological remains (based on Jiménez-Vialás & Grau-Mira, 2019; numbers of archaeological sites refer to the same reference). La Silla del Papa is located just above the upper reaches of the arroyo. Noted is also the longitudinal profile of the Arroyo del Candalar. (c) Upper catchment area with locations of sediment profiles P1 to P9. (d) Overview of the study area (i.e., the low-relief coastal area east of Zahara de los Atunes) from La Silla del Papa; view towards west, Atlantic Ocean in the background. Red lines = topographical transects where terrace levels were documented [Color figure can be viewed at wileyonlinelibrary.com]

FIGURE 3 Overview of the geological setting in the study area (based on Goy et al., 1983). Most of the study area and of the Río del Cachón catchment is dominated by limestones, marls and claystones belonging to the Late Cretaceous Almarchal formation. The upper reaches of the Arroyo del Candalar originate in the Sierra de la Plata, which is composed of Miocene sandstones (Aljibe formation); the transition to the lowlands east of Zahara de los Atunes is indicated by a prominent transpressive fault line along the northern margin of the Sierra de la Plata [Color figure can be viewed at wileyonlinelibrary.com]
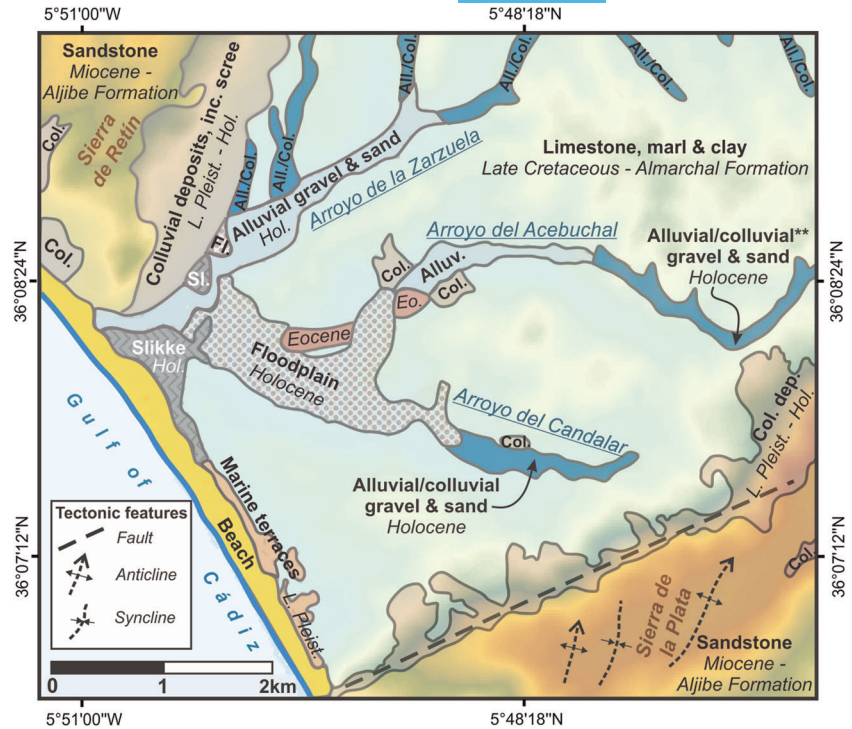
directly below the Iron Age settlement of La Silla del Papa (Figure 2a). With an average slope of 0.78% (Moreno et al., 2010), the floodplain of the main tributaries is agriculturally used, before the Río del Cachón debouches into a small estuary with a closed lagoon north of Zahara de los Atunes. The Arroyo del Candalar is indicated by a typical concave, tripartite longitudinal profile with (i) an upper, erosion-dominated reach; (ii) a middle, transitional reach characterized by a rapidly decreasing channel gradient; and (iii) a lower reach characterized by the accumulation of sediments in a rather wide (up to 500 m) floodplain (e.g., Fryirs & Brierley, 2012; Schumm, 2007).

The coastline is under semidiurnal meso-tidal influence, with mean tidal ranges of 1.25–2.1 m (Gracia et al., 2006; Moreno et al., 2010), neap tides of 0.8 m, and maximum spring tides of approximately 2.6 m (Moreno et al., 2010). According to Gracia et al. (2006), storm waves can reach average heights of 1.5 m. However, the barrier protecting the lagoon is higher than the spring high tide level; accordingly, overwash is only produced during severe storms (and potentially by tsunamis; Moreno et al., 2010).

2.2 | Climatic setting, palaeoenvironmental changes, and sea-level fluctuations

The Mediterranean-Atlantic climate of the area is indicated by mean annual temperatures between 17.2°C and 18.6°C, and mean annual rainfall of c. 550 mm (1981–2010, AEMET, 2018, Moreno et al., 2010), which predominantly occurs during the winter months due to low pressure systems from the Atlantic Ocean (Zazo et al., 2008). The arroyos of this study thus typically are fluvial systems drying out during the summer (torrents). Prevailing winds blow from the west or

the east, with the W/NW-winds being of major importance in wave generation, and E-winds playing a major role in coastal sediment transport (Moreno et al., 2010). The climatic conditions with a pronounced dry season and winter rain result in typical vegetation patterns of the winter-humid subtropics, characterized by a winter-green sclerophyllous tree and bush vegetation, including, among others, *Pistacia lentiscus*, *Quercus coccifera*, *Rosmarinus*, *Cistus* spp. and *Olea europaea* (Reed et al., 2001).

After the Last Glacial Maximum (LGM), relative sea level (RSL) rose to −30/−35 m bsl (below present mean sea level) along the Portuguese and Spanish continental shelves (Dabrio et al., 2000) at the beginning of the Holocene (~10 ka BP). After a period of rapid sea-level rise with rates of 5.7–7 mm year^{-1} until approximately 7 ka BP (Dabrio et al., 2000; Lambeck et al., 2002; Zazo et al., 2008), RSL at the southwestern Iberian coast slowly rose to its present position around 6500 BP, with rates of 2.6–0.9 mm year^{-1} (Boski et al., 2002; Dabrio et al., 2000; Goy et al., 1996; Klein et al., 2016; Vacchi et al., 2016). The maximum inland extent of the transgression is reported to have occurred around 6500 years BP. Related to the rising sea level and in combination with decreasing vertical sedimentation rates, spit-bar barrier systems reflect periods of coastal progradation in the time span approximately 6500–3000 BP and since 2750 years BP until today.

As in other Mediterranean areas, palaeoenvironmental changes in southern Spain are typically documented by changing vegetation patterns and fluctuating soil erosion. Among the reasons for the landscape degradation are successive aridification towards the present semi-arid conditions during the mid-Holocene (Jalut et al., 2009; Pérez-Obiol et al., 2011; Petit-Maire, 1990) and the increasing human impact on vegetation cover and soil by deforestation and

agriculture throughout the entire Holocene (Jalut et al., 2009), combined with generally rough topographies and the abundance of soft sedimentary rocks. However, most of these changes occurred contemporary to the presence of humans, and it remains much debated whether the key drivers for these environmental changes were of climatic origin, by human impact, or result from the combination of both (van Andel & Zangger, 1990; Burillo-Mozota et al., 1986; Bellin et al., 2013; Fuchs et al., 2004; Fuchs, 2007; Roberts, 1990; Roberts et al., 2004, 2011; Schulte, 2002; Vita-Finzi, 1969; Wainwright, 1994; Wolf & Faust, 2015).

In SE Spain, the opening of the landscape and the change towards sclerophyllous vegetation may have started after c. 4400 BP (~2400 BC) during the late Chalcolithic, due to successively increasing dryness and burning, likely combined with intensified pastoralism and forest destruction (Carrión et al., 2010). Here, anthropogenic disturbance (agriculture, mining, deforestation and pastoralism) peaked during and after the Roman occupation. Likewise, Castro et al. (1998) infer human-induced landscape degradation and desertification in SE Spain (Río Aguas) between 6000 BP and 500 BP, that is, between the Late Neolithic and Medieval times. In SW Spain, López-Sáez et al. (2002) presented comparable findings from Cádiz Bay (Lagoon of El Gallo). Based on a multiproxy approach including sedimentary facies analysis, geochemistry, mineralogy, palynology, and micropaleontology, recent investigations on Lake Medina, situated some 60 km to the NNE of the study area, give evidence of arid and warm climatic conditions during the Early Holocene, followed by more humid conditions and highest lake levels between 7800 and 5500 BP, that is, during the Holocene Climatic Optimum (Schröder et al., 2018). Since then, progressive aridification along with the establishment of typical Mediterranean-type vegetation patterns is observed, which is accompanied by increasing anthropogenic impact during the last approximately 2000 years. In addition, studies on varved lake sediments in Zoñar Lake, Andalusia, suggest more humid conditions during the Roman Classical period (Iberian-Roman humid period, ~2600–1600 BP) and drier conditions from 2000 BP onwards (Martín-Puertas et al., 2009), which agrees with other studies reporting wetter conditions in the Mediterranean area at that time (Luterbacher et al., 2006; Roberts et al., 2004; Zanchetta et al., 2007). This humid period, however, was not identified in the Lake Medina record (Schröder et al., 2018), where increased xerophilous and anthropogenic nitrophilous taxa indicate drier, warmer conditions, and elevated human influence, which is in agreement with further marine and lake records (Corella et al., 2011; Moreno et al., 2012) and a trend towards positive NAO values (Olsen et al., 2012).

3 | ARCHAEOLOGICAL SETTING

In the Iberian Peninsula, Neolithic farming societies started to develop approximately 7700 BP (cf. Currás et al., 2012; Jiménez-Guijarro, 2010; Roberts et al., 2011). In the following, five major phases of human occupation are likely to have had a significant impact on the local landscape. First, during the Late Neolithic to Early Bronze Age (before ~3500 BP), the extensive wetlands of the Laguna de la Janda attracted a relatively dense population, which is well documented by rock art manifestations and burial evidence (e.g., Ramos-Muñoz et al., 1998). Second, the transition from the Bronze Age to the Early Iron Age (~900/800 BC), triggered by the foundation of Phoenician trading posts along the Mediterranean and Atlantic coasts of Iberia (such as Kition, Cyprus, 820 BC; Carthage, Tunisia, 814 BC; Mogador, North Africa/Morocco; Cádiz, Andalusia; Abul, Portugal; cf. Aubet, 2001; Marzoli, 2018), led to the appearance of the first proto-urban hillforts known in the area. While a precolonial period with beginning trade-based contact to the indigenous population and a following colonial period with the establishment of settlements was assumed earlier (Aubet, 2001), new chronological data resulted in a re-evaluation of the timing of initial Phoenician colonization in the southern Iberian Peninsula during the last decade (Brandherm, 2006; Núñez-Calvo, 2008). Third, during Iron Age II (~500/200 BC), the consolidation of an urban way of life is observed both in former Phoenician trading posts and in indigenous settlements (García-Jiménez, 2010; Moret, 2004). Then, from the middle of the 1st century BC in the area, the Roman Empire opened a five-century-long period of relative wealth and increasing anthropogenic impact, with the development of larger towns in coastal lowlands (Keay, 1998; Sillières, 1997). Finally, political and economic disturbances during the Late Antiquity forced the population to abandon these lowlands and to reoccupy pre-Roman hilltop settlements (Gutiérrez-Lloret et al., 2017), unlike in the rest of Southern Spain where urban continuity is the rule (Escribano-Paño, 2009; Jiménez-Vialás, 2018 for the nearby Bay of Algeciras).

The hillfort of La Silla del Papa north of Tarifa constitutes a large Iron Age settlement north of the Strait of Gibraltar (Moret et al., 2008, 2010, 2017). It was first occupied during the 9th century BC and, thus, contemporaneous to the Phoenician presence at the coast (Brandherm, 2006; Núñez-Calvo, 2008). Located on the crest of the Sierra de la Plata at 457 m, it persisted during the entire Iron Age and represents the predecessor of the famous Hispano-Roman coastal settlement Baelo Claudia (Moret et al., 2010). While archaeological findings of hand-crafted ceramics and the settlement's location (i.e., hilltop with inland orientation) indicate its indigenous origin, solid evidence for Phoenician and Punic contacts during the following centuries was found before La Silla del Papa was abandoned during the Augustan period and the population moved to Baelo Claudia (Moret & Prados-Martínez, 2014). Recent studies fixed the date of the abandonment to 30–20 BC which corresponds with the foundation of Baelo Claudia (Moret et al., 2017).

Extensive archaeological surveys in the surroundings of La Silla del Papa, including the Zahara Bay area, resulted in a comprehensive picture of the population history in La Silla del Papa and its surrounding territory during the recent past (Jiménez-Vialás & Grau-Mira, 2019). The foundation of small subordinate settlements (Figure 2; Sites 5 and 19) in the low-lying areas of the Zahara valley, located in the NW at the foot slopes of the Sierra de la Plata, seems to have occurred simultaneous to the construction of the hilltop fort.

The number of settlements in the direct vicinity of La Silla del Papa significantly increased during the 4th century BC, including some fortifications and a number of rural sites for agricultural production (i.e., protohistoric farms; Sites 6–8,11,17–18 in Figure 2) that were located on small hills close to small streams and springs in the upper reaches of the arroyos del Candalar and del Acebuchal. After the abandonment of La Silla del Papa in the Augustan period, the number of settlements in the upper reaches of the just mentioned arroyos decreased, although continued agricultural activity is evidenced by two contemporaneous rural agglomerations, villas and/or rural settlements of notable size (Jiménez-Vialás & Grau-Mira, 2019).

In general, romanization involves the introduction of new cultural, political, and economic values and processes that include long-distance market relationships, complex economic systems and exploitation of local resources, that is, agriculture, pasture, mining, water, and forestry (Currás et al., 2012; Hermon, 2008). Therefore, this period is regarded a crucial phase in Holocene landscape changes as activities like deforestation, cropping and intensive agricultural land use, resulted in accelerated soil erosion and, hence, is considered to have had profound environmental impacts (Currás et al., 2012; Walsh, 2004).

4 | METHODS

4.1 | Field work

Field work was carried out between 2015 and 2017. Sediment profiles exposed in natural outcrops (P 1–9) were investigated along the upper reach of the Arroyo del Candalar (Figures 2 and 4). In addition, nine sediment cores (cores C and Z) were drilled in the middle and lower floodplain sections of the Arroyo del Candalar, constituting coring transect A of approximately 3 km length starting close to the estuarine lagoon (Figures 2, 6, and 7).

Coring was performed using an Atlas Copco Cobra vibracoring device with open steel auger heads of 5 and 6 cm outer diameter (Z1–5, C1–4), or closed steel auger heads containing 1 m long PVC tubes of 5 cm diameter (Z6). Sediment profiles and open cores were documented in the field, and sediment samples were generally taken in 3–10 cm intervals representative of the stratigraphy. Closed core Z6 was used for pollen analysis only and was opened in the laboratory (Cologne). All coring sites were measured with a Topcon Hyper Pro DGPS (Differential GPS) with a vertical accuracy of less than or equal to 2 cm. Elevations above or below the present mean sea level (asl/bsl) are based on DGPS measurements of the back-barrier water level of the estuary at Zahara de los Atunes, assumed to represent the mean tidal level.

4.2 | Sedimentological and geochemical analyses

Sedimentary analyses were carried out in the Laboratory for Physical Geography at the University of Cologne. For granulometric and geochemical analyses, the oven-dried (40°C) and hand-pestled sample material was sieved to separate fractions less than or equal to 2 mm (fine fraction) and more than 2 mm (coarse fraction). The fine fraction was taken for further analyses. For grain-size analysis, hydrogen peroxide (H_2O_2; 15%) was added to the samples to remove organic contents, and sodium pyrophosphate ($Na_4P_2O_7$; 47 g/L) was used as a dispersant. Samples were measured using a laser diffraction particle size analyzer (Beckman Coulter LS13320). Grain-size parameters were calculated using GRADISTAT software (Blott & Pye, 2001) and follow the nomenclature of Folk and Ward (1957). For further analyses, the fine-grained fraction was ground using a planetary ball mill (Retsch MM 400). XRF measurements on ground sample material were performed with a portable XRF analytical instrument NITON XL3t 900 GOLDD (Thermo Fisher Scientific). XRF results refer to the average of three measurements and are given in counts. Finally, the Elemental Analyzer vario EL cube (Elementar) was used for the determination of total carbon (TC), total organic carbon (TOC), and total inorganic carbon (TIC) by combustion of sample material in pure oxygen at 950°C. 20 ± 0.5 mg of the ground material were wrapped in tin (TC) or silver (TOC/TIC) containers, respectively. Before the TOC/TIC measurement, the sample material was treated with hydrochloric acid (HCl, 10%) to dissolve inorganic carbon. The results were corrected by a daily factor based on the measurement of a known standard (Acetanilide).

Multivariate statistical analyses were applied for the samples of cores Z1, Z2, Z4, Z5, and C1 (Figure 8) and for samples from P1 to P9 in the form of principal component analysis (PCA), to simplify sedimentological and geochemical results and to determine sedimentary units and depositional facies using the PAST software (Hammer et al., 2001). Parameters were selected based on a prior inspection of the data set. Elements with data discontinuities as well as low concentrations and large errors were excluded, and Spearman's rank correlation coefficient was used to avoid autocorrelations. Variables Fe, Ca, K, mean grain size, and sorting were used for PCA of samples from the floodplain cores ($n = 122$); variables TC, sorting, mean grain size, Fe/Ca, and content of sand were used for PCA of samples from sediment profiles P1–P9 ($n = 56$).

4.3 | Microfaunal and palynological investigations

For microfaunal analyses, 1 cm^3 fresh, non-dried sample material was wet-sieved using a 100 μm mesh. Foraminifers and ostracods were handpicked under a stereoscopic microscope with a minimum of 300 tests per sample. Species identification was based on Cimerman and Langer (1991), Joachim and Langer (2008), Milker and Schmiedl (2012), Pint et al. (2012), Armstrong and Brasier (2005), and the online database WoRMS (World Register of Marine Species) for foraminifers and ostracods. Classification into habitats was based on Murray (2006) for foraminifers and on Meisch (2000), Karanovic (2012) and Pint et al. (2012, 2015) for ostracods (Figure 7).

The closed core Z6 was used for palynological analysis. In total, 15 samples of 1 cm^3 were obtained from the middle section of the
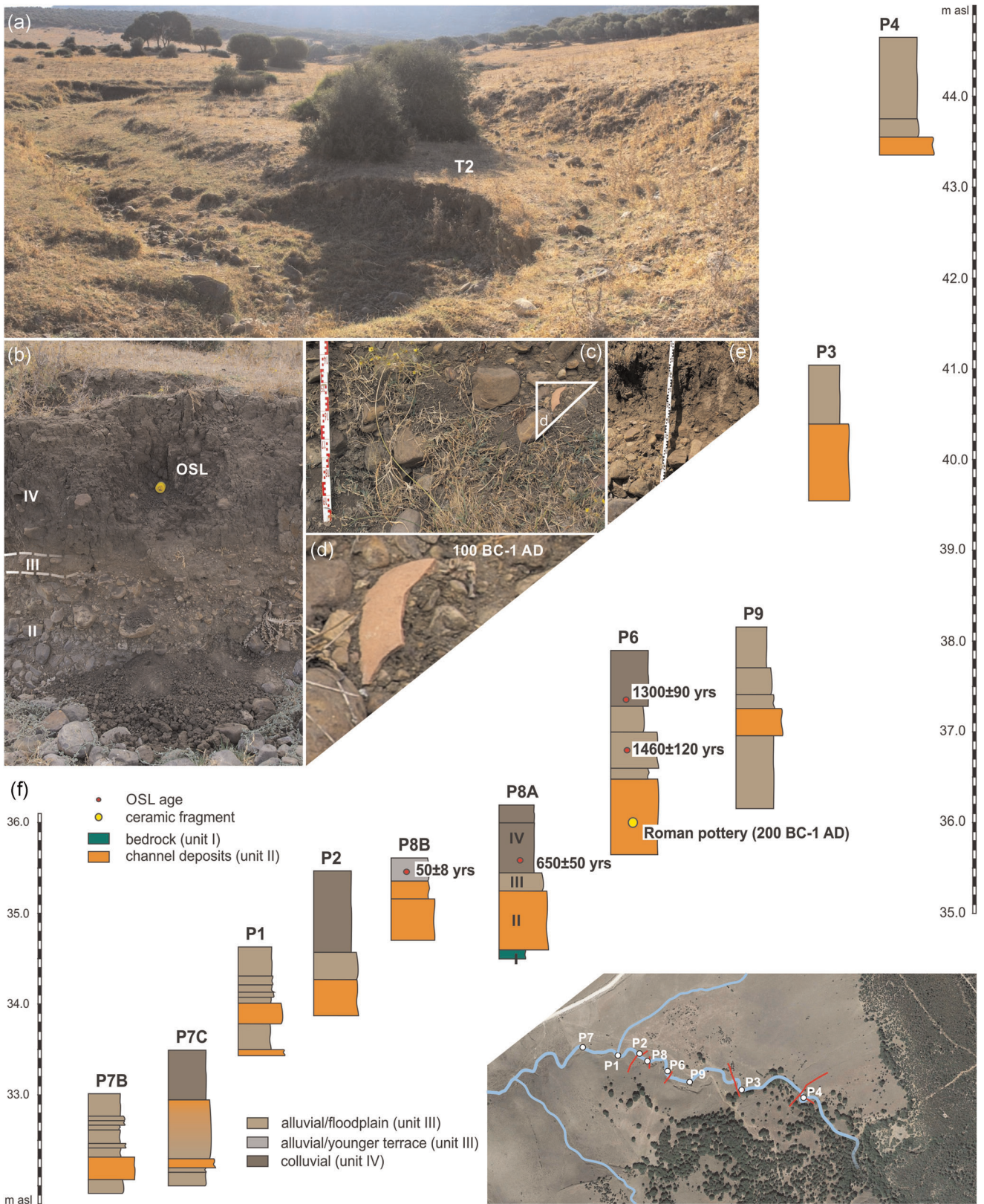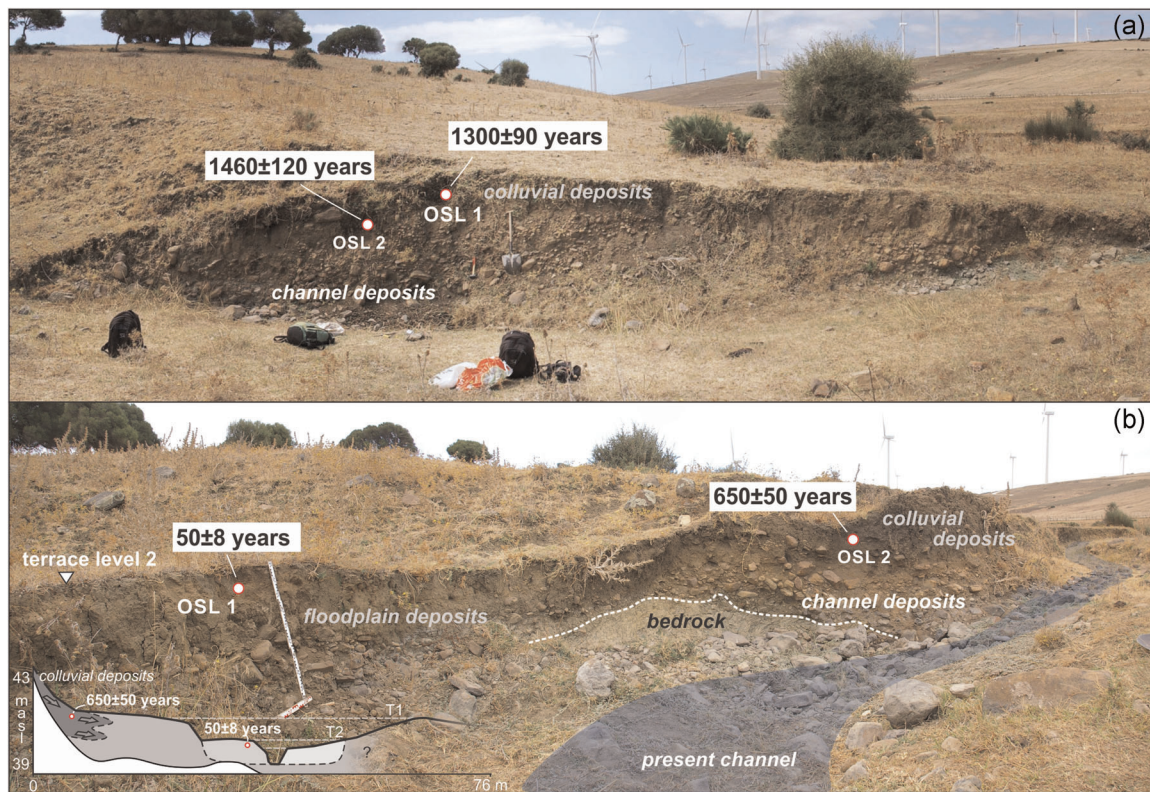
FIGURE 5 Sediment profiles P6 (a) and P8 (b) with OSL ages from colluvial and alluvial units, documented along undercut slopes of the incised river bed. Terrace level 1 is not visible in the photos but is indicated in the schematic sketch shown in (b) [Color figure can be viewed at wileyonlinelibrary.com]

core (5.90–2.26 m b.s.), characterized by gray homogeneous mud. The laboratory treatment included demineralization with cold hydrochloric acid (10%), followed by adding cold hydrofluoric acid (40%) overnight and sieving at 5–6 μm by a nylon mesh using an ultrasound bath (less than 1 min). One tablet with a known number of *Lycopodium* spores (Batch number 1031) was added at the beginning of the preparation to calculate the pollen concentration (Stockmarr, 1971). Prepared subsamples were stored in glycerin and counted under ×400 or ×1000 magnification. Counts of 300 pollen grains per sample were made except for one sample (248 cm) with low pollen concentration. Pollen identification and taxonomy follow Beug (2004) and Moore et al. (1999). Besides pollen and plant spores, nonpollen palynomorphs (NPP), including fungal spores, animal remains, algae, and dinoflagellate cysts as well as charcoal

particles, were identified and counted. For NPP identification, the NPP database (http://nonpollenpalynomorphs.tsu.ru/) was used. Pollen and NPP are expressed as percentages of the total sum of identified pollen (excluding NPP). The diagram (Figure 10) was constructed using the C2 version 1.5.6 (Juggins, 2007). Pollen zonation is based on Constrained Incremental Sums of Squares (CONISS), created for Jaccard indices and justified by the broken stick model using rioja and vegan packages in R.

4.4 | Chronological investigations

The chronological framework is based on ^{14}C-AMS ages (Z1–6, C1–4), Optically Stimulated Luminescence (OSL; P1–9) as well as

FIGURE 4 Sediment profiles P1–9 (P5 not shown) were documented in the transitional reaches of the catchment of the Arroyo del Candalar. The profiles were documented at natural outcrops along the incised channel, located at the transition between the steep and v-shaped valley sections and the ESE-WNW-stretching broader valley. (a) An incipient terrace-like morphology is inferred, that is, bench risers occur at relative elevations of ~1.5 (T2) and 3 m (T1) above the riverbed. (b) OSL sampling on natural outcrops along the channel. The base of all profiles is composed of coarse channel deposits (unit II), followed by alluvial (unit III) and – in most cases – colluvial (unit IV) sediments. Profile height: ~1.5 m (c)–(d) Roman pottery (100 BC-AD 1) was found in the channel deposits of P6. (e) Thick basal coarse channel deposits overlain by fine-grained alluvial deposits. (f) Sequence of sediment profiles along the channel. Coarse channel deposits are found at the base of the profiles (unit II), followed by alluvial (unit III) and – in most cases – colluvial (unit IV) sediments. OSL ages given in years before 2014 [Color figure can be viewed at wileyonlinelibrary.com]
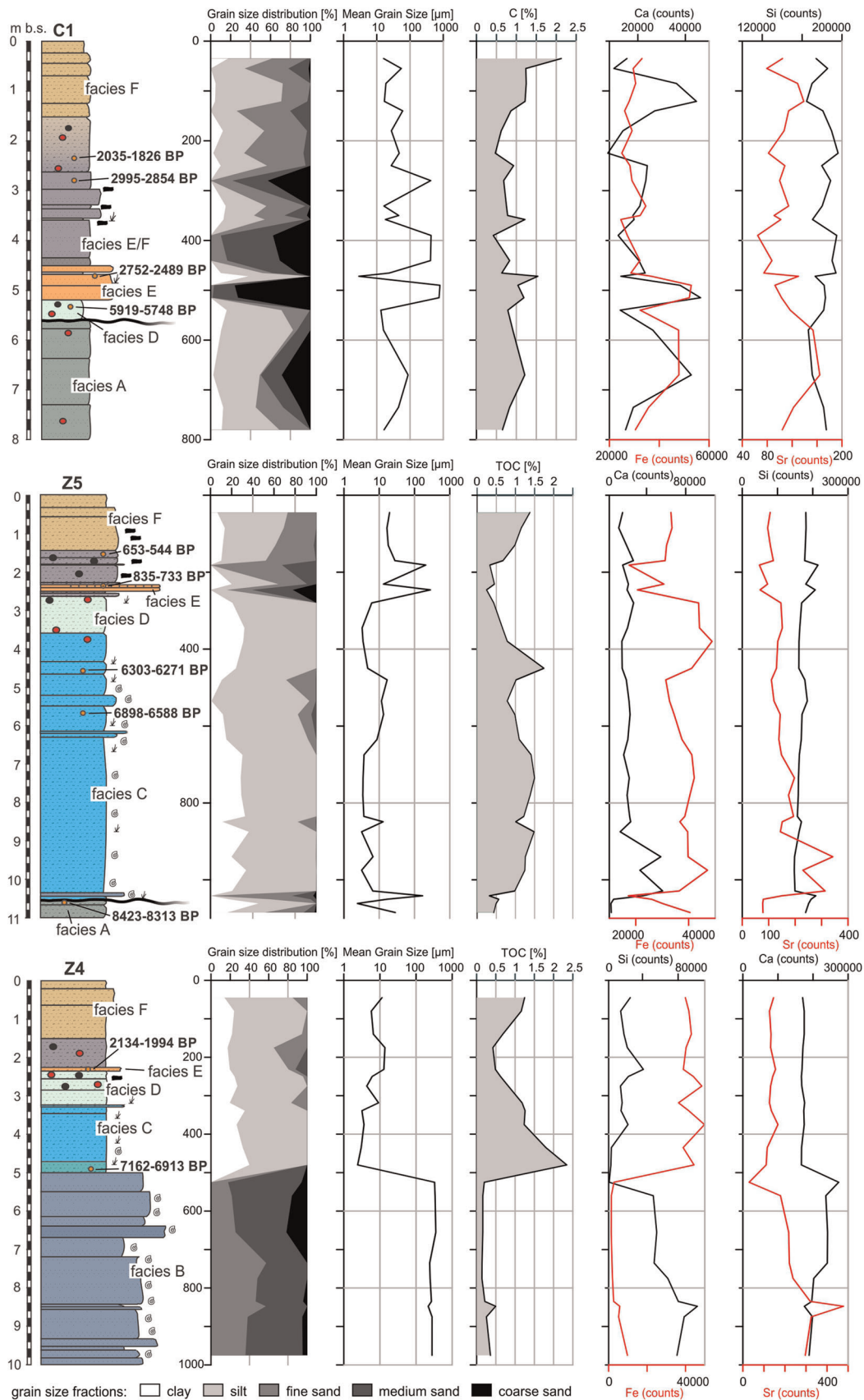
FIGURE 6 Stratigraphy, granulometric results and selected geochemical parameters for master cores C1, Z4, and Z5. For legend of facies/depositional units and further symbols see Figures 7 and 9. ^{14}C-AMS dating results are shown as well [Color figure can be viewed at wileyonlinelibrary.com]
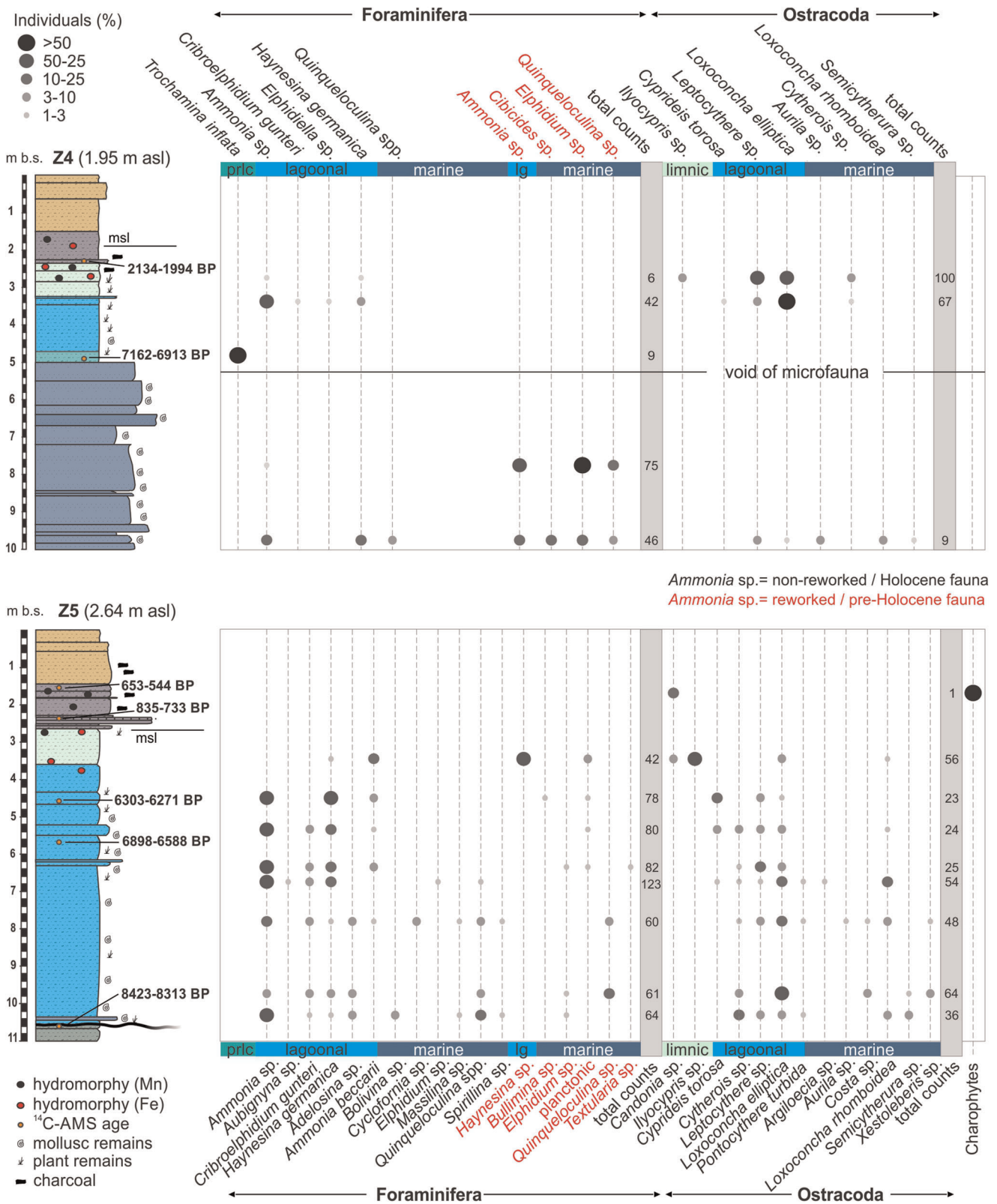
FIGURE 7 Microfaunal results for master cores Z4 and Z5. For legend of facies/depositional units see Figures 6 and 9. ¹⁴C-AMS dating results are shown as well. Prlc – paralic [Color figure can be viewed at wileyonlinelibrary.com]

(a)

(b)
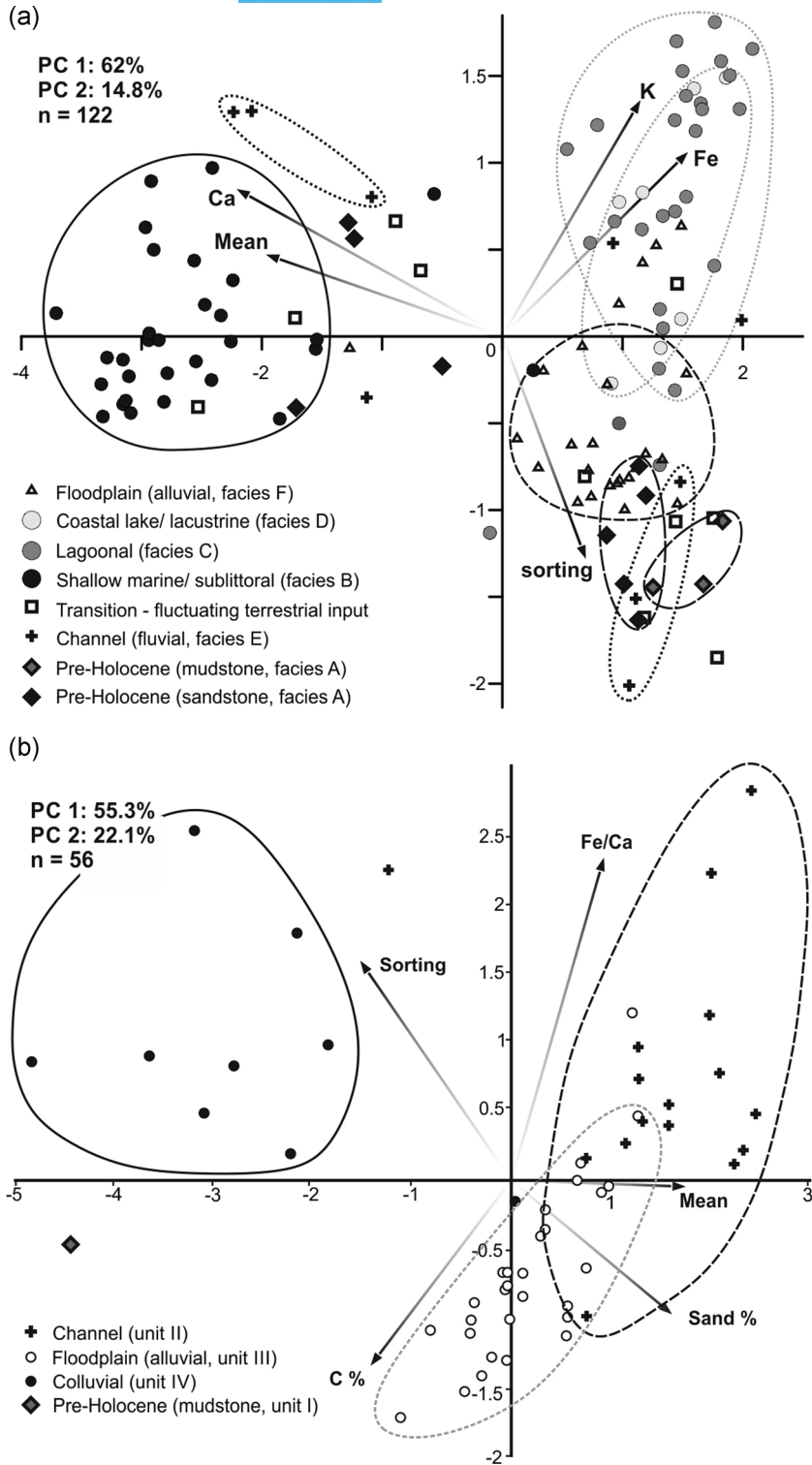
FIGURE 8 Results from PCA of (a) core samples and (b) sediment profiles P1 to P9. (a) PC1 and 2 of the PCA of all sediment samples taken from the cores, together explaining 77% of the variation. Distinct clusters are built by the sublittoral samples of facies B and the fine-grained samples of facies C and D, which are generally separated from the alluvial sediments of facies F. (b) PC1 and 2 of the PCA of sediment samples taken from the sediment profiles P1–P9. While samples from the alluvial and channel units partly overlap, colluvial sediments are clearly separated from the other samples

very few archaeological findings. ^{14}C-AMS analysis was performed at the [14]CHRONO Centre for Climate, the Environment and Chronology, Queen's University Belfast (UK) and Beta Analytic (Miami/FL, USA; samples from closed core Z6). Each sample was calibrated using the INTCAL13 or MARINE13 calibration data sets and Calib 7.1 software (Reimer et al., 2013), and corrected for a local marine reservoir effect of $\Delta R = 40 \pm 15$ (Reimer & McCormac, 2002) where necessary (Table 1).

OSL dating was performed on four sediment samples from P6 and P8 at the Cologne Luminescence Laboratory (CLL) using coarse grain quartz (Table 2). Samples for burial dose determination were collected in steel cylinders pushed horizontally into cleaned trench sections. Pretreatment included sieving, chemical treatment with HCl (10%) and H_2O_2 (10%), density separation (2.62 < quartz < 2.68 g/cm³) and HF etching (40%) was performed under subdued red light to extract the 150–200 μm quartz fraction. Quartz grain aliquots of

TABLE 1 ^{14}C-AMS data

Sample code	Depth (asl/bsl)	Lab. code	Sample material	^{14}C age (BP)	2σ max–min (cal BP)	2σ max–min (cal AD/BC)
Z5/3 + HK	1.34	UBA33445	Charcoal	604 ± 31	653–544	1297–1406 AD
Z5/6 HK	0.29	UBA33447	Charcoal	891 ± 32	910–733	1040–1217 AD
Z5/11 + PR	−1.93	UBA33446	Plant remain	5430 ± 40	6302–6126	4352–4176 BC
Z5/13 + M	−2.96	UBA33448	Closed bivalve[a]	6145 ± 57	[a]6718–6433	4768–4483 BC
Z5/26 PR	−7.85	UBA33449	Plant remains, roots	7552 ± 39	8422–8222	6472–6272 BC
Z4/5 HK	−0.38	UBA35526	Charcoal	2091 ± 27	2134–1994	184–44 BC
Z4/12 PR	−2.85	UBA35528	Wheat grain	6137 ± 41	7162–6913	5212–4963 BC
Z1/9	−1.39	UBA32740	Plant remains, roots	3833 ± 29	4405–4104	2455–2154 BC
Z1/12	−2.20	UBA32741	Plant remains, roots	5638 ± 42	6495–6313	4545–4363 BC
Z1/18	−3.20	UBA32742	Plant remains, wood	5616 ± 37	6469–6309	4519–4359 BC
Z6/1	−5.88	BA573071	Charred plant remains	6160 ± 30	7159–6961 BP	5210–5012 BC
Z6/2	−3.78	BA573072	Charred plant remains	5290 ± 30	6187–5944 BP	4238–3995 BC
Z6/3	−3.30	BA573073	Plant remains (seeds)	4160 ± 30	4828–4579 BP	2879–2630 BC
C1/7	9.74	UBA35529	Charcoal	1980 ± 40	2035–1826	85 BC–AD 124
C1/9	9.29	UBA35530	Charcoal	2818 ± 28	2995–2854	1045–904 BC
C1/16	7.37	UBA35531	Wood remains	2540 ± 44	2752–2489	802–539 BC
C1/18	6.79	UBA35532	Plant remains	5101 ± 34	5919–5748	3969–3798 BC

Note: All ages were calibrated with CALIB 7.1 software and using Reimer et al. (2013).

Abbreviations: asl/bsl above/below present mean sea level; BA, Beta Analytic (Miami/FL, USA); HK, charcoal; Lab. code, laboratory code; M, mollusc shell; PR, plant remains; UBA, ^{14}CHRONO Centre, Queen's University Belfast (UK).

[a]Local marine reservoir effect of ΔR = 40 ± 15 (Reimer & McCormac, 2002).

TABLE 2 Luminescence data and OSL ages for samples from the upper reach of the Arroyo del Candalar

Sample (ZAH-P)	Lab code	Grain size (µm)	Ø (mm)	depth (cm)	$N_{a/m}$	OD (%)	AM	Dose (Gy)	Dose rate (Gy/ka)	Age (years)	Age (AD)
OSL 6-1	CL-4119	150–200	2	16	46/46	11 ± 1	CAM	1.97 ± 0.03	1.53 ± 0.11	1300 ± 90	715 ± 90 AD
OSL 6-2	CL-4120	150–200	2	67	46/46	40 ± 4	MAM	2.13 ± 0.08	1.46 ± 0.10	1460 ± 120	555 ± 120 AD
OSL 8-1	CL-4121	150–200	2	55	94/94	113 ± 8	MAM	0.061 ± 0.01	1.19 ± 0.08	50 ± 8	1965 ± 8 AD
OSL 8-2	CL-4122	150–200	2	110	42/42	64 ± 7	MAM	0.99 ± 0.02	1.53 ± 0.11	650 ± 50	1365 ± 50 AD

Note: The samples were taken in September 2016.

Abbreviations: AM, age model (CAM, central age model; MAM, minimum age model); depth, depth below surface; $N_{a/m}$, number of accepted/measured aliquots; OD, overdispersion; OSL, Optically Stimulated Luminescence.

2 mm diameter were fixed on steel discs using silicon spray, and measured on a Lexyg Research OSL/TL reader equipped with a 90 Sr/90Y beta source delivering ~0.055 Gy/s at the sample position. Signals were stimulated by means of green LEDs and detected through a combination of Schott OG515 (3 mm) and Brightline HC530/43 filters. Equivalent dose measurements were performed using a SAR protocol (Murray & Wintle, 2003) with 10 s preheat at 200°C and a cutheat at 180°C. The appropriateness of the applied protocol was checked by means of a combined dose-recovery preheat-plateau test (preheat plateau at 180–240°C), dose recovery tests (mean dose recovery ratios of 0.99–1.03), and CW-curve fitting (signals dominated by the fast component). For each sample, between 42 and 94 aliquots passed the standard SAR acceptance criteria. Burial dose calculation was based on the central age model (CAM, Galbraith et al., 1999) in case of the well-bleached sample P6-1 (i.e., overdispersion < 20%), and on the minimum age model (MAM, Galbraith et al., 1999) for the incompletely bleached samples P6-2, P8-1, and P8-2 (i.e., overdispersion > 20%). The overdispersion of the best-bleached sample (i.e., 10% for P6-1) was adopted as an estimation for the expected over-dispersion (σb) required for the minimum age model. Dose rate and age calculation were performed using the DRAC software (Durcan et al., 2015), whereas the dosimetry was

based on radionuclide concentrations (uranium, thorium, potassium) in the surrounding sediment derived from high-resolution gamma spectrometry and on in-situ water contents.

5 | RESULTS AND CHRONOSTRATIGRAPHICAL INTERPRETATION

5.1 | Geomorphological observations

Sediment profiles P1–P9 are all located in the transition area between the uppermost, steep and V-shaped valley section of the Arroyo del Candalar and the ESE-WNW-stretching broader valley to the west of the Sierra de la Plata (Figures 2 and 3). This river reach coincides with the well-pronounced slope concavity exhibited in the longitudinal profile (Figure 2a). The break in the riverbed gradient, combined with sufficient accommodation space, induce a sharp decrease in flow velocities and stream power, whereby declining transport capacities result in alluvial deposition. Field observations reveal two main fluvial features along this several hundred meters long reach. First, an incipient meandering pattern is recognized in the narrow (width ~1–2 m) channel bed, which is composed of coarse (pebble) to very coarse (cobble to boulder) material (Figures 4 and 5). Modern concave-bank erosion is witnessed at many places, displaying up to one-meter-high undercut slopes (Figure 5). These natural outcrops exhibit a wide range of grain sizes, from silty to sandy fine-grained sediments up to cobbles and boulders. Second, morphological benches (i.e., small-scale fluvial terraces) are observed above the current channel: they span an elevation difference of up to 3 m and can stretch over several tens of meters in the valley bottom (Figures 4 and 5). They point to an incipient terrace-like morphology, as bench risers are regularly observed at relative elevations of approximately 1.5 (T2) and 3 m (T1) above the riverbed (Figure 4b). At some undercut slopes, rather weathered sedimentary bedrock with folding structures was preserved, likely belonging to the limestones, marls and claystones of the Cretaceous Almarchal Formation (González-Lastras et al., 1991; Figures 4 and 5).

In the lower reaches of the Arroyo del Candalar, the channel is slightly meandering and has incised approximately 1 m into the modern floodplain. Paleochannels occur, especially in the floodplain sections close to the estuary. Between cores C3 and C2, directly upstream of the confluence with the Arroyo del Acebuchal, the floodplain narrows to approximately 100 m width (Figure 2a); due to the alluvial fan formed by the Arroyo del Acebuchal, the channel of the Arroyo del Candalar has shifted to the southern valley side.

5.2 | Sediment profiles in the transitional reach of the catchment

The studied natural outcrops along the transitional reach (sediment profiles P1–P9) are situated at elevations ranging between 33.1 and 44.7 m asl, while their heights range between 0.9 and 2.3 m. Based on
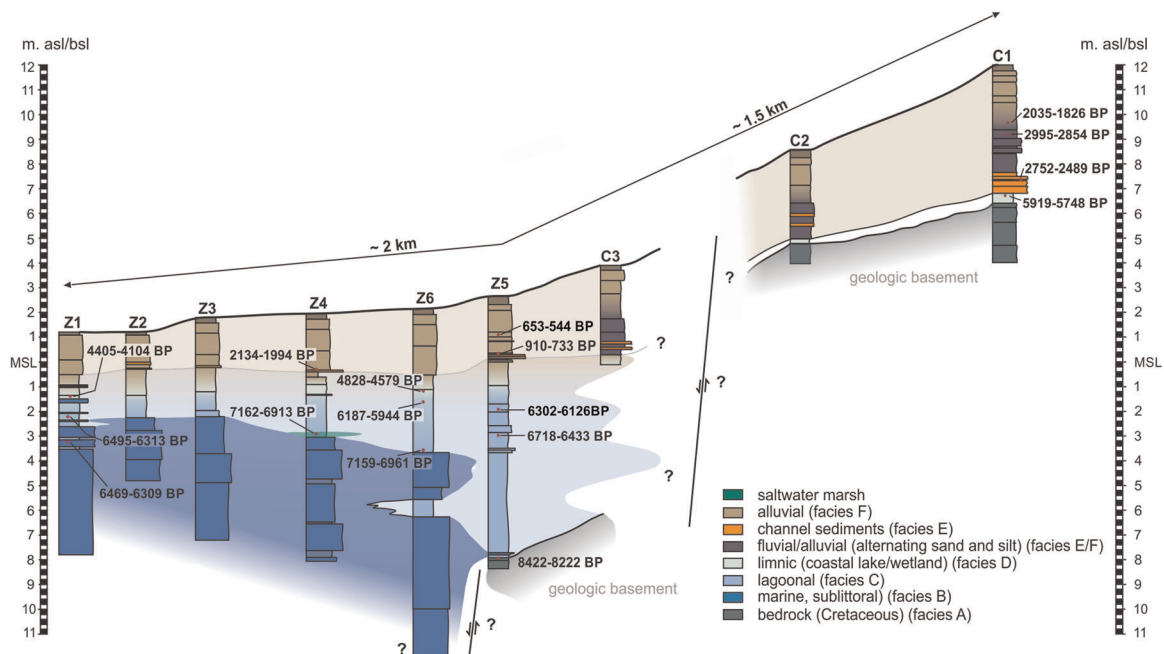
FIGURE 9 Coring transect A, including all cores in the lower floodplain of the Arroyo del Candalar. Between Z5 and C2, the elevations of the basal Cretaceous bedrock units differ by approximately 12–13 m, potentially indicating a fault line. The marine transgression only reached up to the area between Z6 and Z5. The marine strata are covered by a several-meter-thick lagoonal sequence. Then follow terrestrial facies. Palynological analyses were conducted on lagoonal samples from core Z6 (Figure 10). MSL, present mean sea level [Color figure can be viewed at wileyonlinelibrary.com]

the sedimentary characteristics of the samples collected from the sediment profiles as well as the PCA, four main depositional units can be distinguished.

In all profiles (except P8A and B; Figure 4), the exposed sedimentary sequence starts with medium to fine sand with abundant rounded gravels (largest clast ~40 cm in diameter). In the case of P1, P6, and P7C, finer layers of silty sand are interdigitated with these basal layers. The deposits show elevated Fe/Ca ratios and mean grain size values of 460 μm. In addition, they are poorly sorted and have rather low TC values. These units are interpreted as channel-bedload deposits with rather high transport capacities (unit II). Small fluctuations in stream power and channel position account for the presence of finer layers of silty sand intercalating the coarse deposits (P1, P6, and P7C). In profile P6, this basal layer contains a well-preserved fragment of a Roman amphora (at 175 cm b.s.), presumably of pre-Augustan age (200 BC–AD 1; Figure 4).

In contrast, the bottom layer of P8A is characterized by gray color and the absence of any sand components, elevated Al or Ca values, and a relatively high TC value (1.15%). The sample of this unit plots different from all other samples in the PCA (Figure 8b). Despite its weathering grade, the sedimentary rock still displays original folding structures. Thus, this unit I is interpreted as the geologic basement consisting of limestones, marls and claystones (Cretaceous Almarchal Formation; González-Lastras et al., 1991).

Light brown medium to fine sand with average mean grain size values of 270 μm and moderate to poor sorting follows on top of the basal sediment layers of unit II in all profiles. TC values are low (~0.8%) and element values are generally reduced compared with the underlying sediments. This unit III is interpreted as low-energy alluvial deposits, related to final channel deposition and/or to proximal overbanking, which may have accumulated due to decreasing stream powers. In the PCA, unit III builds a separate though overlapping cluster with the channel deposits of unit II (Figure 8b). Deposits from unit III were OSL-dated to 1460 ± 120 years in P6 (P6 OSL2, 110 cm b.s.). In the upper part of P8B, which is related to an intermediate

terrace level, similar deposits were OSL-dated to 50 ± 8 years (at 15 cm b.s., P8B OSL1).

Finally, the upper parts of profiles P2, P6, P7C, P8A, and P8B are characterized by a dark brown color and low mean grain size values of 80 μm on average (unit IV). In comparison to the underlying deposits, these sediments have high mud contents of approximately 30%; their heterogeneity is expressed in very poor sorting. TC values are the highest with approximately 1%, and element values (i.e., Fe and Ca) are also generally high. Deposits of unit IV clearly separate from the other deposits in the PCA (Figure 8b); they are interpreted as colluvial deposits. OSL ages from these deposits in profiles P6 and P8A yielded ages of 1300 ± 90 years (55 cm b.s., P6 OSL 1) and 650 ± 50 years (60 cm b.s., P8A OSL 2), respectively.

5.3 | Sediment cores in the lower floodplain reaches

5.3.1 | Stratigraphy and facies interpretation

Along transect A (Figures 2 and 9), six (Z1–6) plus three (C1–3) sediment cores were retrieved in the floodplain of the lower reaches of the Arroyo del Candalar. Core depths range between 6.0 (Z2) and 14.0 m (Z6), and their elevation above present mean sea level between 1.2 (Z1) and 12.1 m (C1). Cores Z1 and Z2 are both collected from the estuary area, whereas the most inland core C1 is located approximately 4.5 km from the present coastline. While the elevation difference between Z1 and C3 amounts to approximately 2.6 m along a distance of 2.2 km, the floodplain elevation increases to 8.7 m asl between C3 and C2 (distance of ~600 m). Based on the sedimentological and geochemical characteristics of the samples collected from cores Z1–6 and C1–3 as well as the PCA and the microfaunal results, eight different facies can be defined for the sedimentary succession found in the lower floodplain section. The facies represent depositional environments
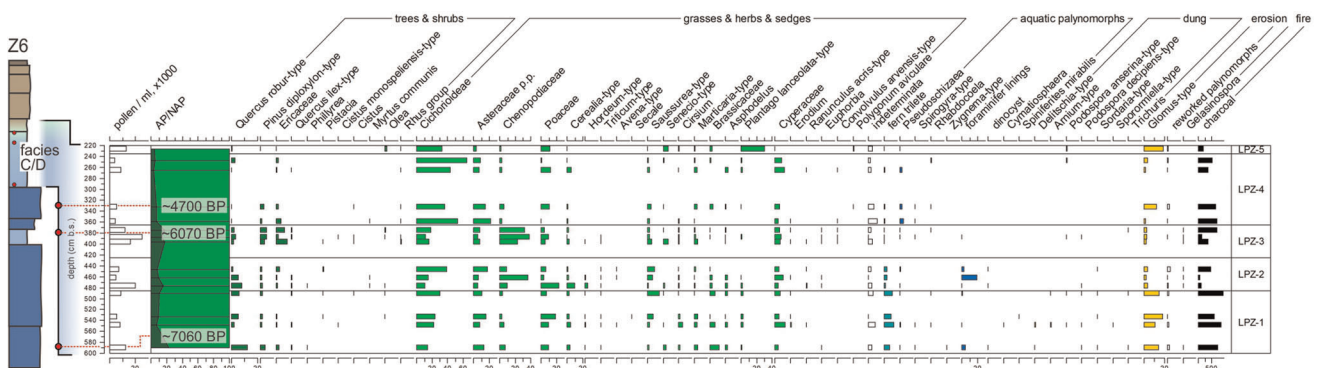
FIGURE 10 Results from the palynological analyses. Altogether five local pollen zones (LPZ1–5) were distinguished. *Quercus robur*-type pollen clearly decrease after LPZ-2, before pine forests represent the dominant arboreal pollen in LPZ-3. Opening of the landscape (deforestation?) is evident in LPZ-4, before Olea-pollen and *Plantago lanceolata*-type pollen increase in LPZ-5. All data are given in %, except for total pollen concentrations. For some samples, the amount of microcharcoal particles is 5 times higher than the amount of pollen grains [Color figure can be viewed at wileyonlinelibrary.com]

that differ in terms of grain size, sorting, organic content, elemental composition, and microfaunal assemblage.

A generally similar sedimentary succession was found for cores Z1–4 and Z6. Gray, moderately to well-sorted medium to fine sand (100%) occurs at the base, with an average mean grain size of 300 μm. High Ca and Si, low Fe, and low TC values (1.6%) are characteristic for these deposits, and samples from this unit cluster due to the high Ca content and mean grain size values (Figures 6 and 8a). Numerous molluscs and mollusc fragments are present. These results point to hydrodynamic conditions with rather high sediment transport capacities, typically found in wave-dominated sublittoral to littoral environments. The interpretation is supported by the presence of reworked foraminifer species, that is, *Ammonia* sp., *Elphidium* spp. and *Quinqueloculina* spp., and autochthonous foraminiferal tests such as *Ammonia* sp., *Haynesina germanica*, and *Quinqueloculina* sp. as well as autochthonous ostracod valves such as *Leptocythere* spp., *Loxoconcha elliptica*, *Aurila* sp., *Loxoconcha rhomboidea*, and *Semicytherura* sp., all of which reflecting the environmental conditions of the littoral zone. Samples from this unit are thus summarized as facies B (marine/sublittoral to littoral; Figure 7). In Z5, the thick sequence of facies B found in the other cores is absent; however, a 10 cm-thin shell debris layer of marine origin was documented just above the basal unit (Figure 6).

The basal unit of Z5 is comprised of highly compacted greenish to grayish brown clayey silt (mud contents ~64%, mean grain size 22 μm on average) with low portions of sand and occasional small stones, exhibiting few organic remains and iron stains. Similar deposits were found at the base of cores C1 and C2. TC values are 0.66% on average. The material is very poorly sorted, Ca values are lowest along the entire transect, and Fe and Si values are comparatively high (Figure 6). These deposits are interpreted as clay- and sandstones of the pre-Holocene bedrock (facies A), that is, the Almarchal Formation (González-Lastras et al., 1991). Samples from these units cluster depending on their sand contents, pointing to internal layering of the bedrock.

Homogeneous grayish brown fine sediments (64 μm on average) with a sand/mud ratio of 20:80 cover the basal sand layers in cores Z1–4 and Z6, as well as the shell debris layer on top of the basal clayey silts at Z5. However, the mean grain size of these deposits ranges between 2.42 μm and 552.6 μm, and the sediments are moderately to poorly sorted. TC values are approximately 1.6%, and Ca values are low, while Fe and K values increase. Numerous plant and root remains, Mn and Fe stains as well as some mollusc shells and mollusc fragments also characterize these sediments. In the PCA, samples from this facies cluster together with the samples from facies D due to its similar sedimentological and geochemical characteristics (Figure 8a). Foraminifer species include *Ammonia* sp. and *Haynesina germanica*, while ostracod species *Cyprideis torosa*, *Leptocythere* sp. and *Loxoconcha elliptica* dominate (Figure 7). These sediments are interpreted as lagoonal deposits (facies C), indicated by still water conditions with reduced wave activity and low current strength.

In most cores (Z1–6 and C3) follow very fine-grained homogeneous deposits with an average mean grain size of 6 μm, with mud

contents of approximately 90% and moderate to poor sorting. Sediments are brown-gray and show average TC values of 1%. While Ca values are similar to those in the underlying deposits, slightly higher Fe values were found. In addition, gastropods, numerous plant remains, few Fe and Mn stains and calcareous concretions are present, indicating the increasing terrestrial influence. Although sediments from this facies cluster together with facies C (Figure 8a), salt-tolerant ostracod species *Candona* sp., *Ilyocypris* sp. and *Loxoconcha elliptica*, as well as the presence of charophytes indicate freshwater to slightly brackish water conditions (Figure 7). These deposits are thus assumed to be of lacustrine origin, that is, representing standing water bodies under increasing freshwater influence, such as a coastal lake evolving from a closed lagoon (facies D). However, the presence of reworked foraminifer species *Haynesina* sp., and autochthonous individuals of *Ammonia beccarii* and *Haynesina germanica* in the lowermost cores suggest sporadic connections to the sea. In cores C1 and C2, similar gray sterile mud deposits were found on top of basal facies A.

Subsequently, a sharp boundary separates the gray mud from the overlying brown sandy deposits in all cores, showing rather high (though fluctuating) mean grain size values around 265 μm; the sand/mud ratio is 60:40 and the sediments are generally poorly sorted. Furthermore, TC values of approximately 1% were found, and Si values increase. Although a separation of samples from this unit remains ambiguous (Figure 8a), these deposits are assumed to be of fluvial (facies E, fluvial/channel deposits) to alluvial (facies F) origin. Facies E is typically well stratified, that is, layers of loamy sand and sandy loam alternate. While the sharp boundary is most prominent in Z5, a clear transition from the underlying mud to the sand-dominated deposits is present in all cores (Figures 6 and 9). As the base of facies E is related to a distinct and in some cases abrupt boundary, erosion during deposition of facies E is assumed, likely related to shifting channel courses and the evolution of a floodplain on top of the fine-grained lagoonal to lacustrine deposits. In Z1, however, alternating fine to medium sand and mud was found instead of the distinct boundary to brown loamy sediments. Here, these sediments are interpreted to reflect fluctuating terrestrial input into a shallow water body, that is, related to an estuary or salt marsh.

Finally, brown and rather compact deposits are found in the upper parts of all cores, though reaching a greater thickness in the landward cores. Mean grain size values are generally low (30 μm), the sand/mud ratio is 40:60, and sediments are poorly sorted. TC and TOC (Z5) values are approximately 1.12% on average and increase towards the top. Samples from this unit cluster in the PCA, although overlapping with deposits from facies C and D as well as facies A. These deposits are summarized as facies F (alluvial/floodplain), reflecting conditions similar to the present ones, that is, the successive accumulation of alluvial deposits (overbank fines) on top of a slightly inclined floodplain. Only a few microfaunal remains, i.e. few individuals of the ostracod species *Candona* sp. and charophytes (Z5, ~170 cm b.s.), were found, suggesting freshwater conditions. In the most seaward core of the transect (Z1), however, non-reworked

individuals of the foraminifera *Ammonia* sp. and the ostracod species *Cyprideis torosa* and *Loxoconcha elliptica* were present (Figure 9).

5.3.2 | Dating results

Plant remains directly on top of facies A in core Z5 (8 m bsl; Figures 6 and 9) were dated by ^{14}C-AMS to 8422–8222 cal BP (Z5/26), just below the marine and lagoonal deposits of facies B and C. Sample Z1/18 from shallow marine facies B yielded an age of 6469–6309 cal BP. At 2.9 m bsl, plant remains from directly above the sand deposits of facies B are 7162–6913 cal BP old (Z4/12). Six samples were taken from the lagoonal mud of facies C; four of them are plant remains (Z5/11: 6302–6126 cal BP; Z1/9: 4405–4104 cal BP; Z1/12: 6495–6313 cal BP; Z6/1: 7159–6961 cal BP), one charred plant material (Z6/2: 6187–5944 cal BP), and one is an undetermined closed bivalve (Z5/13: 6718–6433 cal BP). Finally, sample Z6/3 was taken at the transition to facies D and resulted in an age of 4828–4579 cal BP.

Charcoal fragments from the fluvial and alluvial sediments of facies E and F yield ^{14}C-AMS ages of 2134–1994 cal BP (Z4/5), 910–733 cal BP (Z5/6), and 653–544 cal BP (Z5/3) (Figure 9) in the lower floodplain sections, and 2035–1826 cal BP (C1/7), 2995–2854 cal BP (C1/9), and 2752–2489 cal BP (C1/16) from the same facies at site C1.

5.4 | Palynological results

Pollen analyses of samples taken from facies C and D of core Z6 (i.e., lagoonal and freshwater environments) show high pollen concentrations, a high pollen diversity and a generally moderate to poor pollen preservation decreasing upwards (Figure 10). This is indicated by dominance of Cichorioideae and other Asteraceae, which, due to robust exines, normally get enriched in rather poorly preserved pollen records. The presence of reworked pollen and dinocysts reflects the input of older sediments into the basin from the bottom of the core until 3.32 m b.s. General features of vegetation changes are reflected in the pollen diagram (Figure 10), divided into five local pollen zones (LPZ).

Pollen spectra in the lowermost LPZ-1 (5.90–4.80 m b.s.) show relatively high values of *Quercus robur*-type (up to 13%) and dominance of Cichorioideae (15%–31%), Asteraceae p.p. (9%–17%), and Poaceae (8%–19%). Cerealia-type including *Triticum*-, *Hordeum*-, *Avena*-type, and *Secale* were found, along with *Cirsium*, *Saussurea*-type, *Asphodelus*, Brassicaceae, and *Plantago lanceolata*-type. Coprophilous fungi (*Podospora decipiens*-, *Podospora anserina*-, *Delitschia*, and *Sporormiella*-type) and helminth eggs of *Trichuris* are present. Marine indicators such as foraminifer linings, *Cymatiosphaera* and dinocysts are present together with freshwater indicators *Spirogyra*-type, *Zygnema*-type, and oocytes of Rhabdocoela. The spores of arbuscular mycorrhiza *Glomus*-type reach 19%.

In LPZ-2 (4.80–4.20 m b.s.), Chenopodiaceae (10%–37%) increase, while Asteraceae p.p. (6%–18%) decrease. Within arboreal taxa, decline of *Quercus robur*-type and an increase of Ericaceae are notable at the end of the zone. Cerealia-type reaches a maximum of 11% at 477 cm and then decrease. Coprophilous fungi are presented by *Sordaria* and *Podospora decipiens*-type. Foraminifer linings increase, while freshwater algae are lacking.

Subsequently, LPZ-3 (4.20–3.65 m b.s.) is characterized by an increase in *Pinus diploxylon*-type (5%) and Ericaceae (2%–9%) as well as highest values of Chenopodiaceae (24%–39%). Pollen of garrigue vegetation (*Cistus*, *Pistacia*, *Rhus* group, *Olea*) occur more often. The presence of helminth egg *Trichuris* and coprophilous fungi (*Podospora anserina*-, *P. decipiens*-type) are documented, whereas contents of Cerealia-type pollen decrease. Foraminiferal linings are seldom, while *Spirogyra* and oocytes of Rhabdocoela reappear.

In LPZ-4, (3.65–2.35 m b.s.), a strong decrease of arboreal pollen is evident, together with high contents of Cichorioideae (37%–65%) and Asteraceae p.p. (8%–23%). A maximum of Cerealia-type pollen is found at 2.65 m b.s. *Glomus*-type contents are higher together with the presence of abundant charcoal remains. Spores of coprophilous fungi are rare, while pollen of garrigue vegetation (*Cistus*, *Myrtus communis*, *Rhus* group) as well as *Saussurea*-type, *Matricaria*-type, *Asphodelus*, and *Plantago lanceolata*-type are abundant.

LPZ-5 (2.35–2.20 m b.s.) is presented by one single sample at 2.26 m b.s. Pollen spectra are dominated by *Plantago lanceolata*-type (30%) and Cichorioideae (33%). *Olea* increase to 2%, *Senecio*-type to 4% and *Glomus*-type reaches a maximum of 20%. Spores of *Podospora anserina*-type are present.

6 | DISCUSSION

6.1 | Mid- to late Holocene environmental changes along the Río del Cachón and the Arroyo del Candalar

6.1.1 | Holocene environments, morphodynamic fluctuations, and coastal evolution

In the lowermost reaches of the Arroyo del Candalar, the thick sequence of shallow marine, sublittoral deposits (facies B) in cores Z1–Z4 and Z6 must have accumulated in an open marine embayment. This embayment may have extended up to approximately 2 km landward compared with the present coastline since facies B is almost absent in core Z5, except for the very thin, shell-rich layer at approximately 7.80 m bsl directly overlying the Cretaceous basement (facies A). We, therefore, assume that (sub-)littoral environments likely reached the area of coring location Z5 but not further inland, and that the maximum transgressive extension might have been controlled by the subsurface topography. This is suggested by the clear 13–14 m vertical drop in the top elevation of the Cretaceous bedrock recorded between cores C1–C2 (~5–6 m asl) and Z5 (~8 m bsl) within several hundred meters (Figure 9). However, the cause of this bedrock elevation change remains unclear. Whereas the absence of normal faulting on the geological map seems to preclude a tectonic origin (Figure 3), mass movements in the landslide-prone Cretaceous bedrock or deep erosion during the LGM could be potential explanations.

Finally, the maximum transgression episode in the Zahara Bay occurred at the end of the Early Holocene: the thin marine layer in Z5 was deposited shortly after approximately 8300 cal BP (~6400 cal BC) according to the ^{14}C-AMS age on top of facies A (8 m bsl; Figures 6 and 9). Interestingly, local salt marsh conditions attested by the presence of the foraminifer *Trochamina inflata* at 2.9 m bsl in Z4 are dated at approximately 7100 cal BP (Z4/12; ~5100 cal BC), and the beginning of Facies C at Z6 (3.60 m bsl) at approximately 7060 cal BP (Z6/1; ~5100 cal BC). This implies that shallow marine conditions at Z4 and Z6 ceased around that time, and it points to a rather rapid marine regression in the inner part of the Zahara Bay.

Dominated by *Ammonia* sp. and *Haynesina germanica*, lagoonal conditions of facies C prevailed along the entire Z-transect afterwards. Lagoonal deposits, however, show a clear seaward decreasing thickness. Whereas the latter peaks at more than 5 m in Z5, where it may reflect back-barrier standing water bodies with saltwater influence until at least approximately 6000 cal BP (Z5/11; 4400–4200 cal BC; Z6/2; ~4100 BC), it averages approximately 1 m (or less) in Z1–Z3, where lagoonal conditions persisted longer until at least approximately 4200 BP (~2300 BC) in Z1 (Z1/9; cf. Koster & Reicherter, 2014; Reicherter et al., 2010). In parallel, the elevation of the contact between facies B (marine) and C (lagoonal) slightly increases seaward, possibly suggesting a slowly rising sea level during the inferred seaward advance of the coastline.

The gradual shift from lagoonal facies C to the brackish to lacustrine environments of facies D, likely during the early late Holocene, is supported by the appearance (or dominance; Z5) of the limnic ostracod species *Candona* sp. and *Ilyocypris* sp. (Figure 7). Charred plant material taken from 1.60 bsl in facies D at Z6 dates this transition to around 4700 cal BP (~1.20 m bsl, Z6/3; ~2700 cal BC). In the upper parts of facies D, the presence of oxidation spots points to semi-terrestrial conditions, that is, sediments were likely located around the groundwater level and at least temporarily affected by subaerial conditions.

Along the entire coring transect (C1–3 and Z1–6), the sharp and (in many cases) erosive boundary to the subsequent facies E (fluvial) or F (alluvial) is chronologically constrained to the late Holocene (shortly after 2130–2000 cal BP or 180–40 cal BC, according to the ^{14}C age in Z4). Well-stratified brown sand or loam with numerous hydromorphic features and charcoal fragments give evidence of a sudden shift towards higher morphodynamic activity along the coring transect, likely related to an increased fluvial sediment input, shifting stream channels, and the evolution of the present floodplain, that is, sediment deposition into paleo-wetland environments. Charophyta (Z5) suggest dominating freshwater (or slightly brackish) conditions, and, thus, the termination of saltwater influence, at least in the more landward part of the coring transect.

6.1.2 | Vegetation history and human impact

The dominance of non-arboreal pollen throughout the record is evidence of the presence of open vegetation since at least 7000 BP (~5000 BC). In the lowermost pollen zone LPZ-1, the high values of *Quercus robur*-type indicate patches of open deciduous oak forest and garrigue in the study area during the mid-Holocene, that is, at approximately the time when lagoonal conditions established at site Z6 (~7060 cal BP or 5100 cal BC; Figures 9 and 10). Mediterranean bushes and later temperate forests had developed under relatively humid climatic conditions. This agrees with the results of Schröder et al. (2018), who infer humid conditions and highest lake levels from the sedimentary record of Lake Medina (60 km NNE of the study area) between 7800 and 5500 BP (i.e., ~5800–3500 BC). In addition, foraminifer assemblages, *Cymatiosphaera* and a dinocyst point to an environment with marine influence, that is, a lagoon. The moderate to high contents of Cerealia-type suggest agricultural activities of, among others, barley, wheat, and oat. Pasture activities in the study area are indicated by moderate contents of various coprophilous fungi spores and unpalatable and thorny herbs such as various Asteraceae, *Asphodelus*, and *Euphorbia*. This evidence of agriculture and pasture farming is in line with the occurrence of the first Neolithic settlements in Spain more than 7000 years ago (Jiménez-Guijarro, 2010). Interestingly, sedentism and consolidation of agro-pastoral economies during this period are suggested for the La Janda area, some 12 km north of the study area (Ramos-Muñoz et al., 1998). Additional indirect evidence of an important human settlement in the surroundings of the study area is given by schematic rock art and dolmens in the Sierra de la Plata (Breuil & Burkitt, 1929), as well as a rock shelter (Cueva del Sol; Figure 2b) in close vicinity of the Arroyo del Candalar headwaters, where sun-shaped figures, oculated idols, and even a likely representation of a wheat plant related to the Early Neolithic were found (Sauvet et al., 2014; Versaci-Insúa et al., 2017). In any case, the agricultural activities seem to have resulted in moderate levels of soil erosion, as indicated by the arbuscular mycorrhizal fungus *Glomus*.

In LPZ-2 and LPZ-3, increasing *Pinus diploxylon*-type and Ericaceae values indicate the development of dry pine forests in the study area. Temperate forests seem to have been replaced by pine forests, likely related to the beginning aridification reported from a number of studies in southern Spain, dated to post-5500 BP (~3500 BC; Schröder et al., 2018, Atlantic side) and post-4400 BP (~2400 BC, Carrión et al., 2010, Mediterranean side; Figure 10). This is in general agreement with the ^{14}C-AMS results of sample Z6/2 from the upper part of LPZ-3, which was dated to 6070 cal BP (4100 cal BC), but for which reworking of charred plant material cannot be excluded. On the other hand, studies from Turkey clearly demonstrate pine forest development after 1000 years of intensive land use (i.e., agriculture, pasture, and intense soil erosion) during antiquity, suggesting that these changes can potentially be driven by the human-induced degradation of landscapes (e.g., Shumilovskikh et al., 2016). In the given case, the increase in Chenopodiaceae may point to the presence of salt marshes, whereas a decline in Cerealia-type indicates decreasing agricultural activities, potentially related to the abandonment of small rural settlements and the transfer and/or concentration of population in larger sites such as Los Charcones, Los Algarbes, or

Tarifa, which occurred during the 3rd millennium BC (Costela-Muñoz et al., 2018; Ramos-Muñoz et al., 1998). At the same time, and similar to the microfaunal investigations in core Z5, marine elements such as *Cymatiosphaera*, dinocysts and foraminiferal linings recede, giving additional evidence of the increasing freshwater influence in the standing water bodies of the Zahara Bay and the transition from facies C to facies D.

At the transition to facies D, the strong increase of non-arboreal pollen in LPZ-4 again suggests decreasing forest areas and the spread of open landscapes (e.g., high contents of Cichorioideae, Poaceae, and Asteraceae), while a maximum of Cerealia-type pollen at 2.65 m b.s. is evidence of agriculture. At the same time, chlamydospores of *Glomus*-type show a distinct peak together with the presence of abundant charcoal remains, pointing to increased soil erosion as well as stronger or more frequent fires in the study area. Sample Z6/3 from this core section (i.e., lower to middle part of LPZ-4; charred plant material) dates these changes to post-4700 cal BP (post-2700 cal BC). Spores of coprophilous fungi are rare possibly due to changing depositional conditions, while various Asteraceae, *Asphodelus*, and *Plantago lanceolata*-type suggest the presence of pasture. This generally agrees with the elevated Fe values found in the upper part of facies C and in facies D in Z5, which may tentatively point to increased soil erosion at the time these core sections were deposited (e.g., Brisset et al., 2013; Marriner et al., 2019).

Assuming a possible reworking of the charred material of dating sample Z6/3, the vegetational changes observed in zone LPZ-4 can be attributed to the period of contact with the Phoenicians in Iron Age I or to Iron Age II. Clear evidence, however, is given for forest degradation, increased fire frequency and soil erosion as well as the presence of agriculture and pasture, which is backed by the elevated Fe values in comparable core sections of Z5 (e.g., Marriner et al., 2019). Although potential reasons for this development remain speculative, it may be explained by the presence of an urban settlement at La Silla del Papa since the beginning of the 1st millennium B.C., resulting in increased population along with the foundation of farms and other subordinate settlements in the surrounding area.

In addition, in the very upper part of the core (LPZ-5), the distinct increase in *Olea* may either indicate olive cultivation or the abundance of wild olives in the surroundings of the study area some time before or around 2100 BP (or 180 BC, that is, in the Late Iron Age or Early Roman period). In addition to *Olea*, *Plantago lanceolata*-type strongly increases in this sample as well, along with *Glomus*-type contents, pointing to a rather open landscape. In combination with remains of a torcularium (olive press), found in an Iron Age and Roman site some 4 km to the east of the study area (Grau-Mira & Jiménez-Vialás, 2017), the increase in *Olea* may indeed point to olive plantations, which could likely be related to Early Roman times. Interestingly, these vegetation changes in LPZs 4 and 5 directly precede the deposition of the subsequent fluvial to alluvial sediments, suggesting a temporal correlation of vegetation changes and morphodynamic activity in the catchment area.

6.2 | Implications for the local relative sea-level evolution

The available sample material from the cores in the lower floodplain sections was appropriate for the identification of a few unambiguous sea-level index points (Figure 11; Table 3). The reconstruction of a relative sea-level curve specific for the research area, however, remains challenging. In addition, radiocarbon ages may be biased by the hardwater effect in limestone-dominated areas (Ruello et al., 2017), and—similar to numerous coastal areas in the Mediterranean—these effects cannot be excluded in this study. However, based on the high abundance of *Cyprideis torosa*, *Leptocythere* sp., *Loxoconcha* sp., *Cytherois* sp. as well as the opportunistic species *Haynesina germanica* or *Ammonia* sp., samples from lagoonal facies C may be classified as inner or semi-enclosed lagoon samples according to Vacchi et al. (2016) and others (e.g., Amorosi et al., 2009; Marriner et al., 2012). Rather shallow lagoonal conditions and a deposition close to the lagoonal water table indicated by foraminifers such as *Ammonia* sp., *Elphidiella* sp., and *Haynesina germanica* are most likely. Since the water depth of inner or semi-enclosed lagoons typically remains below 1 m, this environment is assumed to be related to a reference water level (RWL) of −0.5 m, and an indicative range (IR) between mean sea level (MSL) and −1 m (Vacchi et al., 2016). Six samples were taken from the lagoonal mud of facies C; five of these samples derive from plant remains (Z5/11, Z1/9, Z1/12, Z6/1, and Z6/2), and one from an undetermined closed bivalve (Z5/13). Applying the RWL and IR values for inner or semi-enclosed lagoons and an additional error of ± 0.45 m (combined tidal and coring error; cf. Vacchi et al., 2016), the samples represent sea-level index points at approximately 6200 BP (~4250 BC, −1.4 ± 0.95 m), ~6650 BP (~4600 BC, −2.5 ± 0.95 m), ~6400 BP (~4400 BC, −1.7 ± 0.95 m), ~7060 BP (~5100 BC, −3.2 m ± 0.95 m), ~6070 BP (~4100 BC, −1.1 m ± 0.95 m), and ~4200 BP (~2300 BC, −0.9 ± 0.95 m). For sample Z4/12, salt marsh conditions are indicated by the microfaunal results, which are related to an IR between the highest astronomical tide (HAT) and the MSL (Vacchi et al., 2016). With maximum spring tides in the study area of ~2.6 m, we can assign a RWL of 0.65 m and an IR of 1.30 m to sample Z4/12, resulting in a further sea-level index point of −3.5 m ± 1.10 m at approximately 7000 BP (~5100 BC), including tidal and coring errors (Figure 11; Table 3).

Further information can be derived from the terrestrial and marine samples, which can be considered as sea-level limiting points (Vacchi et al., 2016; Figure 11, Table 3). Sample Z5/26 (undetermined root/plant remains) was taken from the uppermost part of facies A, that is, the compacted mudstones of the Cretaceous Almarchal Formation, which contained a thin layer of abundant plant remains and stone fragments. This layer is considered to represent the pre-transgressive surface of the early Holocene valley floor, possibly related to wetland conditions linked to the rising sea level. At approximately 8300 BP (~6400 BC), the local RSL thus must have been located below the position of the sample, that is, below approximately 8 m bsl. In addition, one sample from the shallow marine facies B indicates a minimum RSL position of −3.2 m at approximately
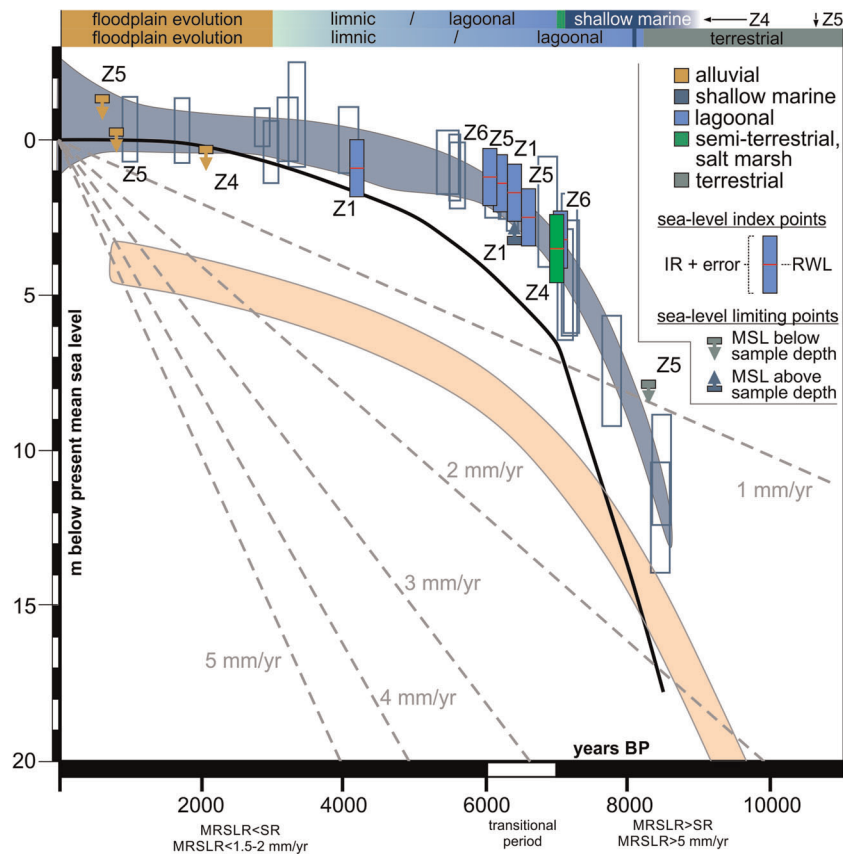
FIGURE 11 Relative sea-level (RSL) curves from the Algarve region compared to sea-level index points and sea-level limiting points used in this study, according to the approach described in Vacchi et al. (2016). Blue area and boxes – RSL curve and sea-level index points based on García-Artola et al. (2018); black line – RSL based on Bradley et al. (2011). Curves are shown together with inferred sedimentation rates (gray dashed lines and orange area; Lario et al., 2002). The sequence of facies for master cores Z4 and Z5 is shown in the upper part of the figure. For the sea-level index points (i.e., samples from lagoonal facies C and the salt marsh in Z4), RSL positions are based on the reference water level (RWL) and the indicative range (IR) plus error assigned to each sample according to Vacchi et al. (2016; cf. also Table 3); arrows indicate the position of respective past sea level (i.e., below or above sample depth) for sea-level limiting points [Color figure can be viewed at wileyonlinelibrary.com]

6400 BP (~4450 BC, Z1/18). Finally, samples from the fluvial or alluvial facies (facies E and F), that is, related to the deposition of channel deposits or overbank fines in the evolving floodplain, are from elevations around or above the former local sea level. Samples Z5/3, Z5/6, and Z4/5 are thus assumed to indicate maximum values for the respective sea level position.

While some minor neotectonic activity (i.e., slow uplift and/or subsidence, < 0.15 mm/a) in the study area during the Holocene cannot be excluded (cf. Grützner et al., 2012), the data points generally agree with existing RSL information as well as curves from the southern Portuguese coast (García-Artola et al., 2018; Teixeira et al., 2005) and the Spanish Atlantic coast (Dabrio et al., 2000; Figure 11). After the early Holocene sea-level rise to −30/−35 m on the Portuguese and Spanish continental shelves (Dabrio et al., 2000), sea level was at −8 m around 8000 BP (or ~6000 BC) according to García-Artola et al. (2018). This is in accordance with the terrestrial plant remain at the base of Z5 dated to ~8300 cal BP (~6400 cal BC), when local RSL at Zahara was lower than 8 m b.s.l. (Figure 11).

Maximum Holocene marine transgression extent in the area is assumed to have occurred at approximately 6500 BP (~4500 BC), and in the following, rapid sea-level rise is thought to have decelerated around 6000 BP (4000 BC) along the Spanish and Portuguese Atlantic coasts, wherefore the rate of sea-level rise decreased from 7 to 5.7 mm year^{-1} between 10,000 and 6500 years BP (8000–4500 BC) to 2.6–0.9 mm year^{-1} thereafter (Dabrio et al., 2000; Zazo et al., 2008; Figure 11). Indeed, the maximum transgression in the Zahara Bay must have occurred after 8300 BP (6400 BC, Z5/26), when a shell-debris layer was deposited at Z5, and before 7000 BP (5000 BC, Z4/12), when salt marsh environments developed at Z4. According to Brisset et al. (2018), this is comparable with the timing of the maximum transgression (~7200 BP) in the western Mediterranean. By then, the coastal zone experienced a metamorphosis from a primary coast (ria-type coast) to a secondary coast (lagoon-barrier coast).

Despite the thin intercalation of marine material at the base of Z5 (evidence of an extreme wave event?), lagoonal environments dominated the area around Z5 shortly after 8300 BP (6400 BC), and

TABLE 3 ^{14}C-AMS data of organic samples and their significance as sea-level index points or sea-level limiting points (cf. Table 1 and Figure 11)

Sample code	Sample depth (asl/bsl)	Significance for sea-level	Assigned RWL	IR	RSL	Tidal and coring errors	2σ max-min (cal BP)	Facies
Z5/3 + HK	1.34	Limiting	MSL	>MSL	<1.34 ± 0.15 m	0.15	653–544	F
Z5/6 HK	0.29	Limiting	MSL	>MSL	<0.29 ± 0.15 m	0.15	910–733	E
Z5/11 + PR	−1.93	Index	−0.5	MSL to −1 m (1 m)	−1.4 m ± 0.95 m	0.45	6302–6126	C
Z5/13 + M	−2.96	Index	−0.5	MSL to −1 m (1 m)	−2.5 m ± 0.95 m	0.45	[a]6718–6433[a]	C
Z5/26 PR	−7.85	Limiting	MSL	>MSL	<−7.85 ± 0.15 m	0.15	8422–8222	A, terrestrial
Z4/5 HK	−0.38	Limiting	MSL	>MSL	<−0.38 ± 0.15 m	0.15	2134–1994	E
Z4/12 PR	−2.85	Index	0.65	HAT to MSL (1.30 m)	−3.5 m ± 1.10 m	0.45	7162–6913	Marsh
Z1/9	−1.39	Index	−0.5	MSL to −1 m (1 m)	−0.9 m ± 0.95 m	0.45	4405–4104	C
Z1/12	−2.20	Index	−0.5	MSL to −1 m (1 m)	−1.7 m ± 0.95 m	0.45	6495–6313	C
Z1/18	−3.20	Limiting	MSL	<MSL	>−3.20 ± 0.15 m	0.15	6469–6309	B
Z6/1	−3.68	Index	−0.5	MSL to −1 m (1 m)	−3.2 m ± 0.95 m	0.45	7159–6961	C
Z6/2	−1.58	Index	−0.5	MSL to −1 m (1 m)	−1.1 m ± 0.95 m	0.45	6187–5944	C

Note: All ages were calibrated with CALIB 7.1 software and using Reimer et al. (2013). asl/bsl above/below present mean sea level. Tidal error = 0.3 m, coring error = 0.15 m according to Vacchi et al. (2016). Abbreviations: IR, indicative range; MSL, mean sea level; RWL, reference water level; RSL, relative sea level elevation = Sample depth − RWL; cf. Vacchi et al. (2016).

[a]Local marine reservoir effect of ΔR = 40 ± 15 (Reimer & McCormac, 2002).

deposits of facies C are found in all cores from 7000 BP (5000 BC) onwards; at that time, local RSL reached approximately 3–2 m bsl, and a rapid seaward progradation of the coastline must have taken place due to sediment accretion (Figure 11), as observed along coastlines in the Mediterranean (Amorosi et al., 1999; Anthony et al., 2014; Gifford et al., 1992). This transition from shallow marine to lagoonal environments in the lower floodplain sections coincides with the decreasing rates of sea-level rise and decreasing sedimentation rates (Figure 11; Dabrio et al., 2000). At that time, littoral dynamics such as longshore drift and barrier evolution likely surpassed the effects of the slowly rising sea level, and coastal barrier systems separated the inner Zahara Bay from the open sea. This corroborates studies on spit-bar systems, pointing to two major periods of coastal progradation, with the older one inferred for the period 6500-3000 BP (or 4500–1000 BC; Dabrio et al., 2000). The younger period of coastal progradation (since 2700 BP or 700 BC) falls in the period of floodplain evolution at Zahara, that is, likely related to human-induced soil erosion, increased sediment availability, and the disappearance of wetlands in the Zahara Bay.

6.3 | Evidence for increased human impact during Roman to post-Roman times?

Two ^{14}C-AMS ages from the lower part of C1 (Figure 8) date to (or shortly after) the transition period from Late Bronze Age to Early Iron Age, with one (2995–2854 BP or 1045–904 BC; C1/9) exactly matching the ^{14}C-AMS date of the first occupation of La Silla del Papa (Moret et al., 2010 and unpublished data). In the surroundings of the Iron Age hillfort, small subordinate rural settlements and later protohistoric farms appeared in the upper reaches of the Arroyo del Candalar during that time (Jiménez-Vialás & Grau-Mira, 2019; Figure 2). In addition, charcoal fragments sampled from destroyed habitat layers, found directly beneath a Visigothic church and Roman tombs southwest of the main settlement of La Silla del Papa, that is, close to the Arroyo del Candalar headwaters, exactly date to the same time period (Moret et al., 2017 and unpublished data). The initiation of increased fluvial activity, related to the infill of sediment traps along the flanks of the Sierra de la Plata, may thus have occurred already during the initial occupation of La Silla del Papa (i.e., during LPZ-4, related to deforestation), merely impacting the floodplain reaches around C1.

However, the main shift recorded during the late Holocene towards the predominance of fluvial dynamics in our small catchment, including floodplain formation in the lowermost floodplain sections, coincides with the Roman and post-Roman period (after 200 BC), which is strongly suggested by some of the ^{14}C ages (e.g., C1 and Z4) as well as OSL ages and Roman pottery (e.g., P6). This observation chronologically matches much broader floodplain aggradation, observed during the same time period in larger river catchments of the Iberian Peninsula (Faust & Wolf, 2017), including those located in the very same region (e.g. Guadalete River). It is traditionally interpreted to be related to a major change in vegetation cover with degradation

of forested areas through massive forest clearing, resulting in remarkable landscape opening and increased soil erosion as can be observed in numerous geological records in the Mediterranean (e.g., Bellin et al., 2013; Carrión et al., 2010; Castro et al., 1998; López-Sáez et al., 2002; Roberts et al., 2011) and around the Strait of Gibraltar (López & Hernández, 2006; Ruiz-Zapata & Gil-García, 2007, 2010). Forest degradation and a simultaneous increase in soil erosion are also inferred from the palynological results of core Z6, i.e. in LPZ-4 and 5 and just below fluvial to alluvial facies E and F, for the time after 4700 cal BP (post-2700 cal BC), thereby directly preceding the period of enhanced fluvial dynamics in the Arroyo del Candalar catchment. This interpretation is additionally supported by the elevated Fe contents documented in the upper part of facies C and in facies D in Z5, which can be regarded as a valuable proxy for soil erosion (e.g., Brisset et al., 2013; Marriner et al., 2019).

In general, the period of enhanced fluvial dynamics in the study area, likely preceded by considerable vegetation changes (increase of *Olea*, *Plantago lanceolata*-type pollen), matches the Roman period. Interestingly, archaeological findings give evidence for a particularly flourishing period related to La Silla del Papa during Roman Republican times, from ca. 150 to 30 BC (Moret et al., 2014, 2017), that is, before the foundation of the Roman city of Baelo Claudia in the Bolonia Bay, some 7 km SE of the study area (Figure 1b; Moret & Prados-Martínez, 2014). With the foundation of Baelo Claudia, it is thought that large parts of the local population moved from the mountains to the coastal plains and that a number of rural settlements (protohistoric farms) in the upper reaches of the Arroyo del Candalar catchment were abandoned, while a few others (i.e., larger rural settlements and villas) were created (Jiménez-Vialás & Grau-Mira, 2019). Whilst it is worth noting that small coastal catchments, such as the one studied here, seem to capture this human-induced signal, it, however, remains unclear whether the increased morphodynamic activity was related to the intensification and/or to changes of agricultural activities during Roman Republican times, or to the abandonment of previously cultivated areas (e.g., Kosmas et al., 2002; Koulouri & Giourga, 2007) during the Augustan era or both. Against the background of the abandonment of several rural settlements in the upper and transitional catchment areas, the abandonment of previously cultivated areas may be considered the more likely explanation in the case discussed here.

As for the upper reach of the Arroyo del Candalar, the basal coarse channel deposits (unit II) in profiles P1–P9 suggest high fluvial dynamics at the foothills of the Sierra de la Plata during or after Roman times, and not earlier (Figure 3). It was followed by a period of floodplain deposition during post-Roman/Early Medieval times (unit III). Shortly after this period and/or parallel to the deposition of the alluvial sediments, colluvial deposits (unit IV), originating from the adjacent hillslopes along the valley, were transported to the lateral channel sections, where they seal the alluvial deposits in some profiles (Figure 3). This is in general agreement with the assumption of a Roman to post-Roman intensification of fluvial activity, as inferred from the lower and middle floodplain reaches, and may suggest reworking of organic material (see the two ^{14}C age inversions

due to the dating of redeposited material in C1). To a certain extent, soil erosion may have been related to the reoccupation of the hillfort site between approximately 600 and 900 AD (i.e., ~1400-1100 BP), which is, amongst others, indicated by the presence of Early Medieval tombs (rock-cut "anthropomorphic" tombs) at mid-elevations in the Sierra de la Plata and surroundings (Grützner et al., 2013; Vargas-Girón, 2011). Finally, based on the OSL age of 50 ± 8 years (OSL 8-1) from terrace Level 2, incision of the uppermost channel section and the formation of the terrace sequence along the upper arroyo reaches occurred during modern times.

Various authors have stressed the significant role of humans on soil erosion intensification and landscape degradation (e.g., Bellin et al., 2013; Fuchs et al., 2004; Fuchs, 2007). While these studies and the results presented here suggest a significant role of human impact on local vegetation composition, sediment availabilities, erosion intensities, and fluvial dynamics, deciphering the contribution of climatic effects – particularly the successive mid- to late Holocene aridification in SW Iberia and its significance for landscape destabilization – remains difficult. As suggested by Wolf and Faust (2015), the combination of increasing land-use pressure and ongoing aridification, and the associated change to the Mediterranean-type periodic pattern of precipitation and discharge, may have transferred landscapes into more fragile environments that were prone to soil erosion and sediment mobility.

7 | CONCLUSIONS

Based on sedimentological, geochemical, chronological, microfaunal, and palynological analyses of nine sediment profiles and nine vibracores, this geoarchaeological study reconstructed mid- to late Holocene environmental changes as well as human–environment interactions in a small river catchment in SW Spain, Andalusia (Río del Cachón). Sediment cores from the lower floodplain sections document an early mid-Holocene open marine embayment, which established at around 8000 BP and reached approximately 2 km inland from the present coastline. The sublittoral deposits are covered by lagoonal and marsh sediments, which expanded from approximately 7000 BP (or ~5000 BC) onwards, likely related to a local regression of the sea and the typical coastal progradation during the late Holocene; this regression may have been promoted by ongoing (though rather low) neotectonic activity in connection with the regional neotectonic setting. Freshwater influence in the coastal wetlands seems to have increased afterwards around 4700 BP, and subsequently, the freshwater-dominated coastal wetlands silted up. Siltation is assumed to be related to increased fluvial and alluvial deposition since ca. 2100 BP, i.e., since the 2nd century BC, which led to the development of the present floodplain in the lower catchment sections. In the transitional reaches of the catchment, coarse channel deposits accumulated around the same time, suggesting that anthropogenic impact on the local landscape was highest during Roman and/or post-Roman times.

Likewise, the palynological results show distinct fluctuations in vegetation patterns since approximately 7000 BP (~5000 BC). Agricultural and pastoral activities, though fluctuating, could be inferred for each of the five LPZs and thus throughout the entire period covered by the sediment core. The results generally point to open vegetation patterns dominated by non-arboreal pollen. However, two distinct periods with clearly reduced contents of arboreal pollen were detected: while temperate forests with patches of deciduous oak were related to rather humid climatic conditions around 7000 BP (5000 BC), a first remarkable opening of the landscape is documented in the subsequent LPZ 2. This period was followed by expanding pine forests, likely related to dryer climatic conditions around or after approximately 6000 BP corroborating other studies. The second period with a remarkable opening of the landscape relates to a decline in the pine forests in LPZ-4, although rather moderate agricultural activities and soil erosion were inferred; while human impact due to agricultural activites is considered moderate during this phase, the remarkable decline of pine forests was dated to post-4700 BP (post-2700 BC) and appears to correspond to the Phoenician and Iron Age period. In contrast, the remarkable increase in *Olea* pollen in the uppermost sample (LPZ-5) may represent the transition to Roman times, shortly before fluvial dynamics and alluvial deposition dominate the lower floodplain of the Arroyo del Candalar.

The increased fluvial and alluvial sedimentation was dated to the last 2100 years when the present floodplain in the lower reaches of the Arroyo del Candalar evolved and substituted wetlands. This was contemporaneous with the abandonment of La Silla del Papa and the foundation of Baelo Claudia, when settlement patterns in the small catchment seem to have changed considerably. The increased sediment availability and sediment transport to the floodplain may have been related to soil erosion and changes in local cultivation techniques, and/or the abandonment of previously cultivated areas at that time. Although the presence of humans and human activities is documented during the entire period, the largest impact—similar to other Mediterranean areas—occurred during Roman or post-Roman times, when increased soil erosion and floodplain sedimentation was inferred.

work and laboratory analyses. We thank two anonymous reviewers for their comments, corrections and suggestions during the review process, which considerably improved the manuscript. The Junta de Andalucía kindly granted the research permits for both the archaeological survey and the geoarchaeological investigations.

ORCID

Simon M. May 🆔 https://orcid.org/0000-0001-6762-7500
Helmut Brückner 🆔 https://orcid.org/0000-0002-2130-5394

REFERENCES

Amorosi, A., Colalongo, M. L., Pasini, G., & Preti, D. (1999). Sedimentary response to Late Quaternary sea-level changes in the Romagna coastal plain (northern Italy). *Sedimentology, 46,* 99–121. https://doi.org/10.1046/j.1365-3091.1999.00205.x

Amorosi, A., Ricci Lucchi, M., Rossi, V., & Sarti, G. (2009). Climate change signature of small-scale parasequences from Lateglacial–Holocene transgressive deposits of the Arno valley fill. *Palaeogeography, Palaeoclimatology, Palaeoecology, 273,* 142–152. https://doi.org/10.1016/j.palaeo.2008.12.010

Van Andel, T. H., & Zangger, E. (1990). Landscape stability and destabilisation in the prehistory of Greece. In S. Bottema, G. Entjes-Nieborg, & W. Van Zeist (Eds.), *Man's Role in the Shaping of the Eastern Mediterranean Landscape* (pp. 139–157). Balkema.

Anthony, E. J., Marriner, N., & Morhange, C. (2014). Human influence and the changing geomorphology of Mediterranean deltas and coasts over the last 6000 years: From progradation to destruction phase? *Earth-Science Reviews, 139,* 336–361. https://doi.org/10.1016/j.earscirev.2014.10.003

Armstrong, H. A., & Brasier, M. D. (2005). *Microfossils.* Blackwell Publishing.

Aubet, M. E. (2001). *The Phoenicians and the West – politics, colonies and trade.* Cambridge University Press.

Bellin, N., Vanacker, V., & De Baets, S. (2013). Anthropogenic and climatic impact on Holocene sediment dynamics in SE Spain: A review. *Quaternary International, 308,* 112–129. https://doi.org/10.1016/j.quaint.2013.03.015

Beug, H.-J. (2004). *Leitfaden der Pollenbestimmung.* Verlag Dr. Friedrich Pfeil (in German).

Blott, S. J., & Pye, K. (2001). GRADISTAT: a grain size distribution and statistics package for the analysis of unconsolidated sediments. *Earth Surface Processes and Landforms, 26,* 1237–1248. https://doi.org/10.1002/esp.261

Boski, T., Moura, D., Veiga-Pires, C., Camacho, S., Duarte, D., Scott, D. B., & Fernandes, S. G. (2002). Postglacial sea-level rise and sedimentary response in the Guadiana Estuary, Portugal/Spain border. *Sedimentary Geology, 150*(1-2), 103–122. https://doi.org/10.1016/S0037-0738(01)00270-6

Bradley, S. L., Milne, G. A., Shennan, I., & Edwards, R. (2011). An improved glacial isostatic adjustment model for the British Isles. *Journal of Quaternary Science, 26*(5), 541–552. https://doi.org/10.1002/jqs.1481

Brandherm, D. (2006). Zur Datierung der ältesten griechischen und phönizischen Importkeramik auf der Iberischen Halbinsel.

Bemerkungen zum Beginn der Eisenzeit in Südwesteuropa. *Madrider Mitteilungen, 47,* 1–23.

Breuil, H., & Burkitt, M. C. (1929). *Rock paintings of southern Andalusia: a description of a Neolithic and Copper age art group* (59 p.). The Clarendon press.

Brisset, E., Burjachs, F., Ballesteros Navarro, B., & Fernández-López, J. (2018). Socio-ecological adaptation to Early-Holocene sea-level rise in the western Mediterranean. *Global and Planetary Change, 169,* 156–167.

Brisset, E., Miramont, C., Guiter, F., Anthony, E. J., Tachikawa, K., Poulenard, J., Arnaud, F., Delhon, C., Meunier, J.-D., Bard, E., & Suméra, F. (2013). Non-reversible geosystem destabilisation at 4200 cal. BP: Sedimentological, geochemical and botanical markers of soil erosion recorded in a Mediterranean alpine lake. *The Holocene, 23,* 1863–1874. https://doi.org/10.1177/0959683613508158

Brückner, H. (1986). Man's impact on the evolution of the physical environment in the Mediterranean region in historical times. *GeoJournal, 13,* 7–17.

Brückner, H., Herda, A., Kerschner, M., Müllenhoff, M., & Stock, F. (2017). Life cycle of estuarine islands – From the formation to the landlocking of former islands in the environs of Miletos and Ephesos in western Asia Minor (Turkey). *Journal of Archaeological Science: Reports, 12,* 876–894. https://doi.org/10.1016/j.jasrep.2016.11.024

Burillo-Mozota, F., Gutiérrez-Elorza, M., Pena-Monne, J. L., & Sancho-Marcen, C. (1986). Quaternary climate in Western Mediterranean. In: F. Lopez-Vera (Ed.). *Proceedings of the Symposium on Climate Fluctuations during the Quaternary in the Western Mediterranean Regions,* Universidad Autonoma, Madrid, pp. 31–44.

Buxó, R. (2008). The agricultural consequences of colonial contacts on the Iberian Peninsula in the first millennium BC. *Veget Hist Archaeobot, 17,* 145–154.

Cammeraat, L. H., & Imeson, A. C. (1998). Deriving indicators of soil degradation from soil aggregation studies in southeastern Spain and southern France. *Geomorphology, 23,* 307–321. https://doi.org/10.1016/S0169-555X(98)00012-9

Carrión, J. S., Fernández, S., Jiménez-Moreno, G., Fauquette, S., Gil-Romera, G., González-Sampériz, P., & Finlayson, C. (2010). The historical origins of aridity and vegetation degradation in southeastern Spain. *Journal of Arid Environments, 74,* 731–736. https://doi.org/10.1016/j.jaridenv.2008.11.014

Castro, P. V., Chapman, R. W., Gili, S., Lull, V., Mico, R., Rihuete, C., Risch, R., Sanahuja, & Yll, E., (1998). *Aguas project. Palaeoclimatic reconstruction and the dynamics of human settlement and land use in the area of the Middle Aguas (Almería) of the Southeast of the Iberian Peninsula.* European Commission environment and climate programme, final Report on Contract EV5V-CT94-0487.

Cimerman, F., & Langer, M. R. (1991). Mediterranean foraminifera. *Slovenska Akademi ja Znanosti in Umetnosti, 30,* 118.

Coltelloni-Trannoy, M., Bridoux, V., & Brouquier-Reddé, V. (2016). Le cercle du Détroit dans l'Antiquité: l'héritage de Miguel Tarradell. *Karthago, 29,* 1–172.

Corella, J. P., Moreno, A., Morellón, M., Rull, V., Giralt, S., Rico, M. T., Peréz-Sanz, A., & Valero-Garcés, B. L. (2011). Climate and human impact on a meromictic lake during the last 6,000 years (Montcortès Lake, Central Pyrenees, Spain). *Journal of Paleolimnology, 46,* 351–367. https://doi.org/10.1007/s10933-010-9443-3

Costela-Muñoz, Y., Castañeda-Fernández, V., Prados-Martínez, F., García-Jiménez, I., & Jiménez-Vialás, H. (2018). La necrópolis de cuevas artificiales de Los Algarbes (Tarifa, Cádiz). Un ejemplo de la permanencia temporal de las construcciones megalíticas. In J. C. Senna-Martínez, M. Diniz, & A. F. Carvalho (Eds.), *De Gibraltar aos Pirenéus. Megalitismo, Vida e Morte na Fachada Atlântica Peninsular* (pp. 481–500). Fundação Lapa do Lobo.

Currás, A., Zamora, L, Reed, J. M., García-Soto, E., Ferrero, S., Armengol, X., Mezquita-Joanes, F., Marqués, M. A., Riera, S., &

Julià, R. (2012). Climate change and human impact in central Spain during Roman times: High-resolution multi-proxy analysis of a tufa lake record (Somolinos, 1280 m asl). *Catena*, 89, 31–53. https://doi.org/10.1016/j.catena.2011.09.009

Dabrio, C. J., Zazo, C., Goy, J. L., Sierro, F. J., Borja, F., Lario, J., González, J. A., & Flores, J. A. (2000). Depositional history of estuarine infill during the last postglacial transgression (Gulf of Cadiz, southern Spain). *Marine Geology*, 162, 381–404. https://doi.org/10.1016/S0025-3227(99)00069-9

Durcan, J. A., King, G. E., & Duller, G. A. (2015). DRAC: Dose Rate and Age Calculator for trapped charge dating. *Quaternary Geochronology*, 28, 54–61.

Escribano-Paño, M. V. (Ed.). (2009). *La investigación sobre la Antigüedad Tardía en España: Estado de los estudios y nuevas perspectivas*. Servicio de Publicaciones de la Diputación de Málaga.

Faust, D., & Wolf, D. (2017). Interpreting drivers of change in fluvial archives of the Western Mediterranean – A critical view. *Earth-Science Reviews*, 174, 53–83. https://doi.org/10.1016/j.earscirev.2017.09.011

Folk, R. L., & Ward, W. C. (1957). Brazos River Bar: A study in the significance of grain size parameters. *Journal of Sedimentary Petrology*, 27, 3–26. https://doi.org/10.1306/74D70646-2B21-11D7-8648000102C1865D

Fryirs, K. A., & Brierley, G. J. (2012). *Geomorphic analysis of river systems: An approach to reading the landscape*. John Wiley & Sons.

Fuchs, M. (2007). An assessment of human versus climatic impacts on Holocene soil erosion in NE Peloponnese, Greece. *Quaternary Research*, 67, 349–356. https://doi.org/10.1016/j.yqres.2006.11.008

Fuchs, M., Lang, A., & Wagner, G. A. (2004). The history of Holocene soil erosion in the Phlious Basin, NE Peloponnese, Greece, based on optical dating. *The Holocene*, 14, 334–345. https://doi.org/10.1191/0959683604hl710rp

Galbraith, R. F., Roberts, R. G., Laslett, G. M., Yoshida, H., & Olley, J. M. (1999). Optical dating of single and multiple grains of quartz from Jinmium rock shelter, northern Australia: Part I, Experimental design and statistical models. *Archaeometry*, 41, 339–364.

García-Artola, A., Stéphan, P., Cearreta, A., Kopp, R. E., Khan, N. S., & Horton, B. P. (2018). Holocene sea-level database from the Atlantic coast of Europe. *Quaternary Science Reviews*, 196, 177–192. https://doi.org/10.1016/j.quascirev.2018.07.031

García-Jiménez, I. (2010). La costa de Tarifa durante el II milenio a.C. y la era de las colonizaciones. Una aproximación a partir de los datos arqueológicos. In F. Prados-Martínez, I. García-Jiménez, & G. Bernard (Eds.), *Confines. El extremo del mundo durante la Antigüedad* (pp. 271–302). Universidad de Alicante.

Gibbons, W. & Moreno, T. (Eds.). (2002). *The Geology of Spain*. London: Geological Society of London.

Gifford, J., Rapp, G., & Vitali, V. (1992). Paleogeography of Carthage (Tunisia): Coastal change during the first millennium BC. *Journal of Archaeological Science*, 19, 575–596. https://doi.org/10.1016/0305-4403(92)90029-3

González-Castillo, L., Galindo-Zaldívar, J., Junge, A., Martínez-Moreno, F. J., Löwer, A., de Galdeano, C. S., Pedrera, A., López-Garrido, A. C., Ruiz-Constán, A., Ruano, P., & Martínez-Martos, M. (2015). Evidence of a large deep conductive body within the basement of the Guadalquivir foreland Basin (Betic Cordillera, S-Spain) from tipper vector modelling: Tectonic implications. *Tectonophysics*, 663, 354–363. https://doi.org/10.1016/j.tecto.2015.08.013

González-Lastras, J., García de Domingo, A., Hernaiz, P. P., Zazo, C., & Goy, J. L. (1991). Cartografía geológica y memoria de la hoja 13–47 (Tarifa). Mapa Geológico de España, Escala 1:50.000. Plan MAGNA, 2ª Serie. IGME, Madrid, Spain.

Goy, J. L., Zazo, C., Dabrio, C. J., Lario, J., Borja, F., Sierro, F. J., & Flores, J. A. (1996). Global and regional factors controlling changes of coastlines in southern Iberia (Spain) during the Holocene. *Quaternary Science Reviews*, 15, 773–780. https://doi.org/10.1016/S0277-3791(96)00071-6

Goy, J. L., Zazo, C., García de Domingo, A., Hernaiz, P. P., & González-Lastras, J. A. (1983). Mapa geológico de España, Escala 1:50.000, Tahivilla, 1074. Inst. Geológico y Min. España.

Gracia, F. J., Alonso, C., Benavente, J., Anfuso, G., & Del-Río, L. (2006). The different coastal records of the 1755 Tsunami waves along the Atlantic Spanish Coast. *Zeitschrift für Geomorphologie*, 146, 195–220.

Grau-Mira, I., & Jiménez-Vialás, H. (2017). *Memoria Final de la Actividad Arqueológica Puntual de Prospección Arqueológica con recogida de materiales y sondeos geoarqueológicos del Proyecto General de Investigación "La Silla del Papa (Tarifa, Cádiz): Oppidum, necrópolis y territorio (2014-2019)"*. Original report in Delegación Provincial de Cultura de Cádiz, pp. 57–60.

Grützner, C., Reicherter, K., Fernández-Steeger, T. M., Müller, D., Verhoeven, S., & Silva, P. G. (2013). Orientation of Visigothic tombs as indicators of recent soil movements and slides: a case study from southern Spain (Betis and Baelo Claudia). In: A. Pastoors, & B. Auffermann (Eds.), *Pleistocene foragers: Their culture and environment*. Festschrift in honour of Gerd - Christian Weniger for his sixtieth birthday. Wissenschaftliche Schriften des Neanderthal Museums, 6; Mettmann.

Grützner, C., Reicherter, K., Hübscher, C., & Silva, P. G. (2012). Active faulting and neotectonics in the Baelo Claudia area, Campo de Gibraltar (southern Spain). *Tectonophysics*, 142, 554–557. https://doi.org/10.1016/j.tecto.2012.05.025

Grützner, C., Reicherter, K., & Silva, P. G. (2010). Comparing semiquantitative logic trees for archaeoseismology and palaeoseismology: The Baelo Claudia (southern Spain) case study. *GSA Spec*, 471, 1–18.

Gutiérrez-Lloret, S., Lefebvre, B., & Moret, P. (2017). La iglesia altomedieval de la Silla del Papa (Tarifa, Cádiz). *Mélanges de la Casa de Velázquez*, 47(1), 203–216.

Hammer, Ø., Harper, D. A., & Ryan, P. D. (2001). PAST: Paleontological statistics software package for education and data analysis. *Palaeontologia Electronica*, 4(1), 9.

Hermon, E. (2008). *Vers une gestion intégrée de l'eau dans l'Empire romain*. Actes du colloque international, Université Laval, octobre 2006 (Vol. 16). L'Erma di Bretschneider.

Jalut, G., Dedoubat, J. J., Fontugne, M., & Otto, T. (2009). Holocene circum-Mediterranean vegetation changes: climate forcing and human impact. *Quaternary international*, 200, 4–18. https://doi.org/10.1016/j.quaint.2008.03.012

Jiménez-Guijarro, J. (2010). Cazadores y campesinos. La Neolitización del interior de la Península Ibérica. Bibliotheca Archaeologica Hispana, 31. Madrid: Real Academia de la Historia

Jiménez-Vialás, H. (2018). Los paisajes que encontró Tariq. La bahía de Algeciras entre los siglos III y VIII. *Lucentum*, 37, 251–269. https://doi.org/10.14198/LVCENTVM2018.37.14

Jiménez-Vialás, H., & Grau-Mira, I. (2019). From pre-Roman Bailo to Roman Baelo: Long-term landscape dynamics in the Straits of Gibraltar. *Oxford Journal of Archaeology*, 38, 228–246. https://doi.org/10.1111/ojoa.12166

Joachim, F., & Langer, M. R. (2008). *The 80 most common ostracods from the Bay of Fetoveia, Elba Island (Mediterranean Sea)*. Selbstverlag Universität Bonn.

Juggins, S. (2007). *C2 version 1.5 user guide. Software for ecological and palaeoecological data analysis and visualisation*. Newcastle University.

Karanovic, I. (2012). *Recent fresh water Ostracods of the World. Crustacea, Ostracoda, Podocopida*. Springer.

Keay, S. (1998). The development of towns in early Roman Baetica. In S. Keay (Ed), The Archaeology of Early Roman Baetica. (Journal of Roman Archaeology Supplement, 29) Portsmouth, US., pp. 55-83.

Klein, T., Bebermeier, W., Krause, J., Marzoli, D., & Schütt, B. (2016). Sedimentological evidence of an assumed ancient anchorage in the

hinterland of a Phoenician settlement (Guadiana estuary/SW-Spain). *Quaternary International*, 407, 110–125. https://doi.org/10.1016/j.quaint.2015.12.038

Kosmas, C., Danalatos, N. G., López-Bermúdez, F., & Romero-Díaz, M. A. (2002). The effect of land use on soil erosion and land degradation under Mediterranean conditions. In N. A. Geeson, C. J. Brandt, & J. B. Thornes (Eds.), *Mediterranean desertification: A mosaic of processes and responses*, pp. 57–70.

Koster, B., & Reicherter, K. (2014). Sedimentological and geophysical properties of a ca. 4000 year old tsunami deposit in southern Spain. *Sedimentary Geology*, 314, 1–16. https://doi.org/10.1016/j.sedgeo.2014.09.006

Koulouri, M., & Giourga, C. (2007). Land abandonment and slope gradient as key factors of soil erosion in Mediterranean terraced lands. *Catena*, 69, 274–281. https://doi.org/10.1016/j.catena.2006.07.001

Lambeck, K., Yokoyama, Y., & Purcell, T. (2002). Into and out of the Last Glacial Maximum: sea-level change during Oxygen Isotope Stages 3 and 2. *Quaternary Science Reviews*, 21, 343–360. https://doi.org/10.1016/S0277-3791(01)00071-3

Lario, J., Zazo, C., Goy, J. L., Dabrio, C. J., Borja, F., Silva, P. G., Sierro, F., González, A., Soler, V., & Yll, E. (2002). Changes in sedimentation trends in SW Iberia Holocene estuaries (Spain). *Quaternary International*, 93–94, 171–176. https://doi.org/10.1016/S1040-6182(02)00015-0

Luterbacher, J., Xoplaki, E., Casty, C., Wanner, H., Pauling, A., Küttel, M., Rutishauser, T., Brönnimann, S., Fischer, E., Fleitmann, D., Gonzalez-Rouco, F. J., García-Herrera, R., Barriendos, M., Rodrigo, F., Gonzalez-Hidalgo, J. C., Saz, M. A, Gimeno, L., Ribera, P., Brunet, M., ... & Ladurie, E. L. R. (2006). Mediterranean climate variability over the last centuries: A review. *Developments in Earth and Environmental Sciences*, 4, 27–148. https://doi.org/10.1016/S1571-9197(06)80004-2

López-Sáez, J. A., García, P. L., & Sánchez, M. M. (2002). Palaeoecology and Holocene environmental change from a saline lake in South-West Spain: Protohistorical and prehistorical vegetation in Cádiz Bay. *Quaternary International*, 93, 197–206. https://doi.org/10.1016/S1040-6182(02)00018-6

López-García, P., & Hernández-Carretero, A. M. (2006). Análisis de pólenes. In: Roldán, L., Bendala, M., Blánquez, J., & Martínez, S. (Eds.), *Estudio histórico-arqueológico de la ciudad de Carteia (San Roque, Cádiz). 1994-1999 (Arqueología Monografías, 24, vol. II, CD).* Madrid: Consejería de Cultura de la Junta de Andalucía, Universidad Autónoma de Madrid, pp. 1–7.

Marriner, N., Gambin, T., Djamali, M., Morhange, C., & Spiteri, M. (2012). Geoarchaeology of the Burmarrad ria and early Holocene human impacts in western Malta. *Palaeogeography, Palaeoclimatology, Palaeoecology*, 339, 52–65. https://doi.org/10.1016/j.palaeo.2012.04.022

Marriner, N., Kaniewski, D., Gambin, T., Gambin, B., Vannière, B., Morhange, C., Djamali, M., Tachikawa, K., Robin, V., Rius, D., & Bard, E. (2019). Fire as a motor of rapid environmental degradation during the earliest peopling of Malta 7500 years ago. *Quaternary Science Reviews*, 212, 199–205. https://doi.org/10.1016/j.quascirev.2019.03.001

Martín-Puertas, C., Valero-Garcés, B. L., Brauer, A., Mata, M. P., Delgado-Huertas, A., & Dulski, P. (2009). The Iberian–Roman Humid Period (2600–1600 cal yr BP) in the Zoñar Lake varve record (Andalucía, southern Spain). *Quaternary Research*, 71, 108–120. https://doi.org/10.1016/j.yqres.2008.10.004

Marzoli, D. (2012). Neugründungen im phönizischen Westen. Los Castillejos de Alcorrín, Morro de Mezquitilla und Mogador. *Archäologischer Anzeiger*, 2, 29–64. https://publications.dainst.org/journals/aa/121/4806

Marzoli, D. (2018). Rencontres entre Orient et Occident: les Phéniciens le long des côtes de la péninsule Ibérique et du Maroc. *Dialogues d'histoire Ancienne*, 44/1, 225–251.

Marzoli, D., Gonzaléz-Wagner, C., Suárez-Padilla, J., Mielke, D. P., López-Pardo, F., León-Martín, C., Thiemeyer, H., & Torres-Ortiz, M. (2009). Vorbericht zu den deutsch-spanischen Ausgrabungen in der endbronzezeitlichen Siedlung von Los Castillejos de Alcorrín, Manilva (Prov. Málaga) 2006 und 2007. *Madrider Mitteilungen*, 50, 118–148.

Marzoli, D., González-Wagner, C., Suárez-Padilla, J., López-Pardo, F., León-Martín, C., Thiemeyer, H., & Torres-Ortiz, M. (2010). Los inicios del urbanismo en las sociedades autóctonas localizadas en el entorno del Estrecho de Gibraltar: investigaciones en Los Castillejos de Alcorrín y su territorio (Manilva, Málaga). *Menga: Revista de Prehistoria de Andalucía*, 1, 153–183.

Marzoli, D., Suárez-Padilla, J., & Torres-Ortiz, M. (2014). Die Meerenge von Gibraltar am Übergang von der Bronze- zur Eisenzeit (9.-8. Jh. v. Chr.). Zum Forschungsstand. *Madrider Mitteilungen*, 55, 167–211.

Meisch, C. (2000). *Süßwasserfauna von Mitteleuropa*. Spektrum Akademischer Verlag.

Milker, Y., & Schmiedl, G. (2012). A taxonomic guide to modern benthic shelf foraminifera of the western Mediterranean Sea. *Palaeontologia Electronica*, 15(2), 16A 1–134. https://doi.org/10.26879/271

Moore, P. D., Webb, J. A., & Collinson, M. E. (1999). *Pollen analysis*. Blackwell Science.

Moreno, A., Pérez, A., Frigola, J., Nieto-Moreno, V., Rodrigo-Gámiz, M., Martrat, B., González-Sampériz, P., Morellón, M., Martín-Puertas, C., Corella, J. P., Belmonte, Á., Sancho, C., Cacho, I., Herrera, G., Canals, M., Grimalt, J. O., Jiménez-Espejo, F., Martínez-Ruiz, F., Vegas-Vilarrúbia, T., & Valero-Garcés, B. L. (2012). The medieval climate anomaly in the Iberian peninsula reconstructed from marine and lake records. *Quaternary Science Reviews*, 43, 16–32. https://doi.org/10.1016/j.quascirev.2012.04.007

Moreno, I. M., Ávila, A., & Losada, M. Á. (2010). Morphodynamics of intermittent coastal lagoons in Southern Spain: Zahara de los Atunes. *Geomorphology*, 121, 305–316. https://doi.org/10.1016/j.geomorph.2010.04.028

Moret, P. (2004). Premieres formes d'urbanisme dans l'Iberie du second age du Fer. In S. Agusta-Boularot, & X. Lafon (Eds.), *Des Ibères aux Vénètes* (Vol. 328, pp. 133–157). Collection de l'Ecole Francaise de Rome.

Moret, P., Fabre, J. M., García-Jiménez, I., Prados-Martínez, F., & Constans, A. (2010). La Silla del Papa (Tarifa, Cádiz): Bilan de trois années de recherches. *Pallas*, 82, 441–463.

Moret, P., Muñoz-Vicente, Á., García-Jiménez, I., Callegarin, L., Michel, O., Fabre, J.-M., Prados-Martínez, F., & Rico, C. (2008). La Silla del Papa (Tarifa, Cádiz): Aux origines de Baelo Claudia. *Mélanges de la Casa de Velázquez. Nouvelle série*, 38-1, 353–367.

Moret, P., & Prados-Martínez, F. (2014). Les deux Baelo: du site perché protohistorique au site portuaire romain sur la rive nord du détroit de Gibraltar. In L. Mercuri, R. Gonzalez, & F. Bertoncello (Eds.), *Implantations humaines en milieu littoral méditerranéen: facteurs d'installation et processus d'appropriation de l'espace (Préhistoire, Antiquité, Moyen Âge)* (pp. 137–148). Antibes.

Moret, P., Prados-Martínez, F., Fabre, J. M., Fernández-Rodríguez, E., García-Fernández, F. J., Gonzalez, F., & Jiménez-Vialás, H. J. (2017). La Silla del Papa: hábitat y necrópolis. Campañas 2014-2016. *Mélanges de la Casa de Velázquez. Nouvelle série*, 47-1, 49–71.

Moret, P., Prados-Martínez, F., García-Jiménez, I., & Muñoz-Vicente, A. (2014). El oppidum de Bailo/Silla del Papa y el Estrecho de Gibraltar en tiempos de Sertorio. In F. Sala, & J. Moratalla (Eds.), *Las guerras civiles romanas en Hispania. Una revisión histórica desde la Contestania* (pp. 141–153). Universidad de Alicante; Museo Arqueologico de Alicante.

Murray, A. S., & Wintle, A. G. (2003). The single aliquot regenerative dose protocol: potential for improvements in reliability. *Radiation Measurements*, 37, 377–381.

Murray, J. W. (2006). *Ecology and Applications of Benthic Foraminifera*. Cambridge University Press.

Núñez-Calvo, F. (2008). Western Challenges to East Mediterranean Chronological Frameworks. In: D. Brandherm, & M. Trachsel (Eds.), *A New Dawn for the Dark Age? Shifting Paradigms in Mediterranean Iron Age Chronology*. Proceedings of the XV Congress of the UISPP. Colloquium C53. Lisboa 4–9 September 2006 (Oxford 2008), 3–27.

Olsen, J., Anderson, N. J., & Knudsen, M. F. (2012). Variability of the North Atlantic Oscillation over the past 5,200 years. *Nature Geoscience*, 5, 808–812.

Petit-Maire, N. (1990). Natural aridification or man-made desertification? A question for the future. In R. Paepe, R. W. Fairbridge, & S. Jelgersma (Eds.), *Greenhouse effect, sea level and drought* (pp. 281–285). Springer.

Pint, A., Frenzel, P., Fuhrmann, R., Scharf, B., & Wennrich, V. (2012). Distribution of *Cyprideis torosa* (Ostracoda) in Quaternary athalassic sediments in Germany and its application for palaeoecological reconstructions. *International Review of Hydrobiology*, 97(4), 330–335.

Pint, A., Seeliger, M., Frenzel, P., Feuser, S., Erkul, E., Berndt, C., Klein, C., Pirson, F., & Brückner, H. (2015). The environs of Elaia's ancient open harbor – A reconstruction based on microfaunal evidence. *Journal of Archaeological Science*, 54, 340–355.

Pérez-Obiol, R., Jalut, G., Julià, R., Pèlachs, A., Iriarte, M. J., Otto, T., & Hernández-Beloqui, B. (2011). Mid-Holocene vegetation and climatic history of the Iberian Peninsula. *The Holocene*, 21, 75–93. https://doi.org/10.1177/0959683610384161

Ramos-Muñoz, J., Domínguez-Bella, S., Morata-Céspedes, D., Pérez-Rodríguez, M., Montañés-Caballero, M., Castañeda-Fernández, V., Herrero-Lapaz, N., & García-Pantoja, M. E. (1998). Aplicación de las técnicas geoarqueológicas en el estudio del proceso histórico entre el V y III milenios A.N.E. en la comarca de la Janda (Cádiz). *Trabajos de Prehistoria*, 55, 163–176.

Reed, J. M., Stevenson, A. C., & Juggins, S. (2001). A multi-proxy record of Holocene climatic change in southwestern Spain: The Laguna de Medina, Cádiz. *The Holocene*, 11, 707–719. https://doi.org/10.1191/09596830195735

Reicherter, K., Vonberg, D., Koster, B., Fernández-Steeger, T., Grützner, C., & Mathes-Schmidt, M. (2010). The sedimentary inventory of tsunamis along the southern Gulf of Cádiz (southwestern Spain). *Zeitschrift für Geomorphol. Suppl. Issues*, 54, 147–173. https://doi.org/10.1127/0372-8854/2010/0054S3-0023

Reimer, P. J., Bard, E., Bayliss, A., Beck, J. W., Blackwell, P. G., Bronk Ramsey, C., Buck, C. E., Cheng, H., Edwards, R. L., Friedrich, M., Grootes, P. M., Guilderson, T. P., Haflidason, H., Hajdas, I., Hatt, C., Heaton, T. J., Hogg, A. G., Hughen, K. A., Kaiser, K. F., ... & van der Plicht, J. (2013). IntCal13 and MARINE13 radiocarbon age calibration curves 0–50000 years cal BP. *Radiocarbon*, 55(4), 1869–1887.

Reimer, P. J., & McCormac, F. G. (2002). Marine radiocarbon reservoir corrections for the Mediterranean and Aegean Seas. *Radiocarbon*, 44(1), 159–166.

Renzi, M., Bode, M., & Marzoli, D. (2016). Ausbeutung von Bergbauressourcen im Umland von Los Castillejos de Alcorrín (Manilva, Málaga) (Ende 9. und 8. Jh. v. Chr.). Ein Vorbericht. *Madrider Mitteilungen*, 57, 139–211.

Renzi, M., Marzoli, D., Suárez-Padilla, J., & Bode, M. (2014). Estudio analítico de los materiales arqueometalúrgicos procedentes de Los Castillejos de Alcorrín (Manilva, Málaga). yacimiento del Bronce Final/Inicios de la Edad del Hierro en el entorno del Estrecho de Gibraltar. *Madrider Mitteilungen*, 55, 121–166.

Roberts, N. (1990). Human-induced landscape change in south and southwest Turkey during the later Holocene. In S. Bottema, G. Entjes-Nieborg, & W. van Zeist (Eds.), *Man's Role in the Shaping of the Eastern Mediterranean Landscape* (pp. 53–67). Balkema.

Roberts, N., Brayshaw, D., Kuzucuoğlu, C., Perez, R., & Sadori, L. (2011). The mid-Holocene climatic transition in the Mediterranean: Causes and consequences. *The Holocene*, 21, 3–13. https://doi.org/10.1177/0959683610388058

Roberts, N., Stevenson, T., Davis, B., Cheddadi, R., Brewster, S., & Rosen, A. (2004). Holocene climate, environment and cultural change in the circum-Mediterranean region. In R. W. Battarbee, F. Gasse, & C. E. Stickley (Eds.), *Past Climate Variability through Europe and Africa* (pp. 343–362). Springer.

Ruello, M. R., Cinque, A., Di Donato, V., Molisso, F., Terrasi, F., & Ermolli, E. R. (2017). Interplay between sea level rise and tectonics in the Holocene evolution of the St. Eufemia Plain (Calabria, Italy). *Journal of Coastal Conservation*, 21(6), 903–915.

Ruiz-Zapata, M. B., & Gil-García, M. J. (2007). Análisis polínico de la fábrica de salazones: avance de las investigaciones. In A. Arévalo, & D. Bernal (Eds.), *Las cetariae de Baelo Claudia. Avance de las investigaciones arqueológicas en el barrio meridional (2000-2004) (Arqueología Monografías* (pp. 513–520). Cádiz: Junta de Andalucía, Universidad de Cádiz.

Ruiz-Zapata, M. B., & Gil-García, M. J. (2010). El medio ambiente. Análisis polínico de las factorías de Traducta. In R. Bernal, & D. Jiménez-Camino (Eds.), *Las cetariae de salazones de Iulia Traducta. Resultados de las excavaciones arqueológicas en la calle San Nicolás de Algeciras (2001-2006)* (pp. 497–502). Universidad de Cádiz.

Sauvet, G., González-Sainz, C., Sanchidrián, J. L., & Villaverde, V. (2014). Europe: Prehistoric rock art. In C. Smith (Ed.), *Encyclopedia of Global Archaeology* (pp. 2599–2612). Springer. https://doi.org/10.1007/978-1-4419-0465-2_1278

Schröder, T., van't Hoff, J., López-Sáez, J. A., Viehberg, F., Melles, M., & Reicherter, K. (2018). Holocene climatic and environmental evolution on the southwestern Iberian Peninsula: A high-resolution multi-proxy study from Lake Medina (Cádiz, SW Spain). *Quaternary Science Reviews*, 198, 208–225. https://doi.org/10.1016/j.quascirev.2018.08.030

Schulte, L. (2002). Climatic and human influence on river systems and glacier fluctuations in southeast Spain since the Last Glacial Maximum. *Quaternary International*, 93, 85–100. https://doi.org/10.1016/S1040-6182(02)00008-3

Schumm, S. A. (2007). *River variability and complexity*. Cambridge University Press.

Shumilovskikh, L. S., Seeliger, M., Feuser, S., Novenko, E., Schlütz, F., Pint, A., Pirson, F., & Brückner, H. (2016). The harbour of Elaia: A palynological archive for human environmental interactions during the last 7500 years. *Quaternary Science Reviews*, 149, 167–187. https://doi.org/10.1016/j.quascirev.2016.07.014

Sillières, P. (1997). *Baelo Claudia. Una ciudad romana de la Bética*. Casa de Velázquez.

Silva, P. G., Goy, J. L., Zazo, C., Bardají, T., Lario, J., Somoza, L., Luque, L., & González-Hernández, F. M. (2006). Neotectonic fault mapping at the Gibraltar Strait Tunnel area, Bolonia Bay (South Spain). *Engineering Geology*, 84, 31–47. https://doi.org/10.1016/j.enggeo.2005.10.007

Stockmarr, J. (1971). Tablets with spores used in absolute pollen analysis. *Pollen et Spores*, 13, 615–621.

Teixeira, S. B., Gaspar, P., & Rosa, M. (2005). Holocene sea-level index points on the Quarteira coast (Algarve, Portugal) In M.C. Freitas, T. Drago (Eds.), *Iberian Holocene Paleoenvironmental Evolution*. Proceedings Coastal Hope Conference 2005, Universidade de Lisboa, Lisboa, pp. 125–127.

Thornes, J., & Brandt, C. J. (Eds.). (1996). *Mediterranean Desertification and Land Use*. Wiley.

Thornes, J. B., & Wainwright, J. (2004). Environmental issues in the Mediterranean: Processes and Perspectives from the Past and Present. Routledge, 512 pages.

Tsetskhladze, G. R. (2006). Greek Colonisation: An Account of Greek Colonies and Other Settlements Overseas, *Greek Colonisation: an account of greek colonies and other settlements overseas* (Vol. 1). Leiden.

Vacchi, M., Marriner, N., Morhange, C., Spada, G., Fontana, A., & Rovere, A. (2016). Multiproxy assessment of Holocene relative sea-level changes in the western Mediterranean: Sea-level variability and improvements in the definition of the isostatic signal. *Earth-Science Reviews*, 155, 172–197. https://doi.org/10.1016/j.earscirev.2016.02.002

Vargas-Girón, J. M. (2011). El fenómeno funerario rupestre en el Campo de Gibraltar. Un estado de la cuestión. *Almoraima: Revista de estudios campogibraltareños*, 42, 143–165.

Vergés, J., & Fernández, M. (2012). Tethys–Atlantic interaction along the Iberia–Africa plate boundary: The Betic–Rif orogenic system. *Tectonophysics*, 579, 144–172. https://doi.org/10.1016/j.tecto.2012.08.032

Versaci-Insúa, M., González Martínez-Pais, I., Lazarich, M., Torres-Abril, F., Carreras-Egaña, A., Galindo del Pozo, M., & Pardo de Donlebún, S. (2017). La Cueva del Sol, un marcador solar en la Sierra de la Plata (Tarifa, Cádiz). *SPAL – Revista de Prehistoria y Arqueología*, 26, 295–310.

Vita-Finzi, C. (1969). *The Mediterranean Valleys: Geological Changes in Historical Times*. Cambridge University Press.

Wainwright, J. (1994). Anthropogenic factors in the degradation of semi-arid regions: A prehistoric case study in Southern France. In A. C. Millington, & K. Pye (Eds.), *Effects of environmental change on drylands* (pp. 285–304). John Wiley and Sons.

Walsh, K. (2004). Caring about sediments: the role of cultural geoarchaeology in Mediterranean landscapes. *Journal of Mediterranean Archaeology*, 17, 223–245.

Wolf, D., & Faust, D. (2015). Western Mediterranean environmental changes: Evidences from fluvial archives. *Quaternary Science Reviews*, 122, 30–50. https://doi.org/10.1016/j.quascirev.2015.04.016

Zanchetta, G., Drysdale, R. N., Hellstrom, J. C., Fallick, A. E., Isola, I., Gagan, M. K., & Pareschi, M. T. (2007). Enhanced rainfall in the Western Mediterranean during deposition of sapropel S1: stalagmite evidence from Corchia cave (Central Italy). *Quaternary Science Reviews*, 26(3-4), 279–286.

Zazo, C., Dabrio, C. J., Goy, J. L., Lario, J., Cabero, A., Silva, P. G., Bardají, T., Mercier, N., Borja, F., & Roquero, E. (2008). The coastal archives of the last 15ka in the Atlantic–Mediterranean Spanish linkage area: Sea level and climate changes. *Quaternary International*, 181, 72–87. https://doi.org/10.1016/j.quaint.2007.05.021

Zazo, C., Silva, P. G., Goy, J. L., Hillaire-Marcel, C., Ghaleb, B., Lario, J., Bardají, T., & González, A. (1999). Coastal uplift in continental collision plate boundaries: Data from the Last Interglacial marine terraces of the Gibraltar Strait area (south Spain). *Tectonophysics*, 301, 95–109. https://doi.org/10.1016/S0040-1951(98)00217-0